(2)

TECHNICAL REPORT RD-GC-88-22

STRUCTURAL MODE FREQUENCIES OF FOG-M ACTUATOR/FIN

Gordon D. Welford
Guidance and Control Directorate
Research, Development, and Engineering Center

NOVEMBER 1988

U.S. ARMY MISSILE COMMAND
Redstone Arsenal, Alabama 35898-5000

Cleared for public release; distribution is unlimited.

DISPOSITION INSTRUCTIONS

DESTROY THIS REPORT WHEN IT IS NO LONGER NEEDED. DO NOT RETURN IT TO THE ORIGINATOR.

DISCLAIMER

THE FINDINGS IN THIS REPORT ARE NOT TO BE CONSTRUED AS AN OFFICIAL DEPARTMENT OF THE ARMY POSITION UNLESS SO DESIGNATED BY OTHER AUTHORIZED DOCUMENTS.

TRADE NAMES

USE OF TRADE NAMES OR MANUFACTURERS IN THIS REPORT DOES NOT CONSTITUTE AN OFFICIAL INDORSEMENT OR APPROVAL OF THE USE OF SUCH COMMERCIAL HARDWARE OR SOFTWARE.

UNCLASSIFIED

SECURITY CLASSIFICATION OF THIS PAGE

REPORT DOCUMENTATION PAGE

Form Approved
OMB No 0704-0188
Exp Date Jun 30 1986

1a. REPORT SECURITY CLASSIFICATION UNCLASSIFIED	1b. RESTRICTIVE MARKINGS
2a. SECURITY CLASSIFICATION AUTHORITY	3. DISTRIBUTION / AVAILABILITY OF REPORT Cleared for public release; distribution is unlimited.
2b. DECLASSIFICATION / DOWNGRADING SCHEDULE	
4. PERFORMING ORGANIZATION REPORT NUMBER(S) Tech Report RD-GC-88-22	5. MONITORING ORGANIZATION REPORT NUMBER(S)
6a. NAME OF PERFORMING ORGANIZATION Guidance & Control Directorate Res, Dev, & Eng Center 6b. OFFICE SYMBOL (If applicable) AMSMI-RD-GC-C	7a. NAME OF MONITORING ORGANIZATION
6c. ADDRESS (City, State, and ZIP Code) Commander, U.S. Army Missile Command ATTN: AMSMI-RD-GC-C Redstone Arsenal, AL 35898-5254	7b. ADDRESS (City, State, and ZIP Code)
8a. NAME OF FUNDING / SPONSORING ORGANIZATION 8b. OFFICE SYMBOL (If applicable)	9. PROCUREMENT INSTRUMENT IDENTIFICATION NUMBER
8c. ADDRESS (City, State, and ZIP Code)	10. SOURCE OF FUNDING NUMBERS PROGRAM ELEMENT NO. / PROJECT NO. / TASK NO. / WORK UNIT ACCESSION NO

11. TITLE (Include Security Classification)

STRUCTURAL MODE FREQUENCIES OF FOG-M ACTUATOR/FIN

12. PERSONAL AUTHOR(S)
Gordon D. Welford

13a. TYPE OF REPORT	13b. TIME COVERED	14. DATE OF REPORT (Year, Month, Day)	15. PAGE COUNT
	FROM Oct 84 TO Dec 84	1988 November	41

16. SUPPLEMENTARY NOTATION

17. COSATI CODES			18. SUBJECT TERMS (Continue on reverse if necessary and identify by block number)
FIELD	GROUP	SUB-GROUP	Control Actuation Systems; Bending Modes; Control Fins; Mechanical Stiffness

19. ABSTRACT (Continue on reverse if necessary and identify by block number)

An earlier report examined the pneumatic servo stiffness as a potential cause of marginal fin flutter mode stability. In this analysis, the bending stiffness of the vane, vane actuator shaft, vane and actuator bearing combination is examined. It is shown that there exists a predominant 50 Hz mode which is caused by the fin structure and the radial type spring of the fin base into which the actuator shaft is inserted.

20. DISTRIBUTION / AVAILABILITY OF ABSTRACT ☐ UNCLASSIFIED/UNLIMITED ☒ SAME AS RPT ☐ DTIC USERS	21. ABSTRACT SECURITY CLASSIFICATION UNCLASSIFIED
22a. NAME OF RESPONSIBLE INDIVIDUAL Gordon D. Welford	22b. TELEPHONE (Include Area Code) (205) 876-1225 22c. OFFICE SYMBOL AMSMI-RD-GC-C

DD FORM 1473, 84 MAR 83 APR edition may be used until exhausted
All other editions are obsolete

SECURITY CLASSIFICATION OF THIS PAGE
UNCLASSIFIED

ACKNOWLEDGEMENT

The author wishes to acknowledge the following people for their contributions during the laboratory investigation part of this analysis:

Carl H. Warren
William W. Malcolm
Roger P. Berry
J. C. Dunnaway
Mark Dixon
Don A. Hall

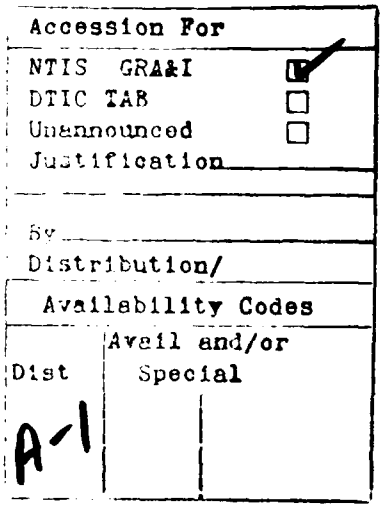

TABLE OF CONTENTS

LIST OF ILLUSTRATIONS

LIST OF ILLUSTRATIONS (Continued)

I. INTRODUCTION

This report was originally published as an internal Letter Report (RG-10-85, 20 Dec 84). The question of servo stiffness and stability for the small second generation actuator was addressed in an internal report.[1] In MIL Flight No. 6, where the large second generation actuator was used, there was again a "hint" of the flutter phenomenon when several short bursts of 48 Hz, 4.2° P-P limit cycles appeared on the Vane No. 2 potentiometer signal. This appeared at both low and high Q conditions, with the frequency being the same. There was nothing in the servo stiffness analysis which would indicate a soft spot or preference for a frequency in the 50 Hz range. In this analysis, the bending stiffness of the vane, vane/actuator shaft, vane mounting, and actuator bearing combination are examined. There is definitely a predominant structural mode in the 50 Hz range. The particular fins used in this laboratory test were fins No. 5 and No. 3* as identified in Table 1. Fin No. 5 has a steel base structure which has been mass balanced to locate the center of mass very close to the axis of rotation. Fin No. 3* used in the wind tunnel tests was unbalanced and has an aluminum base structure. Note that the control fins used in MIL No. 6 were only partially mass balanced about the hinge axis. Thus, there was ample room for coupling bending motion orthogonal to the actuator shaft axis into the observed rotational motion.

The "limit cycle" bursts noted in MIL Flight No. 6 were not particularly troublesome. However, in the interest of long range (perhaps production) design robustness and the desirability of using the lower cost non-mass-balanced fins, this analysis was made to try to isolate the primary contributor to the 50 Hz range bending mode. Henceforth this bending mode, which can actually vary from 42 Hz to 53 Hz depending on the shaft/fin interface, will be referred to as the 50 Hz mode.

[1] Servo Stiffness Analysis of the Second Generation FOG-M Pneumatic Actuator, Letter Report RG-13-85, 10 Dec 84.

TABLE 1. Control Fin Inertia and CG Data

Fin No.	Weight (lb)	Distance From CG to Trailing Edge (in.)	Moment of Inertia About CG ($in.^2$-lb)	Moment of Inertia About Hinge Axis ($in.^2$-lb)
1	0.505	2.03	0.244	0.268
2	0.447	2.03	0.216	0.237
3	0.515	2.08	0.265	0.280
4	0.445	2.01	0.217	0.243
5	0.550	2.19	0.284	0.286
6	0.425	1.98	0.202	0.233
1*	0.345	1.75	0.122	0.192
3*	0.290	1.75	0.103	0.162

NOTES:

1. Distance from the hinge axis to trailing edge is 2.25 in.

2. Fin Nos. 1 and 4 were used on MIL Flight No. 6 and were partially mass balanced about the hinge axis.

3. Fin Nos. 5 and 6 were used for wind tunnel testing and were partially mass balanced about the hinge axis.

4. Fin Nos. 1* and 3* are unbalanced and represent pre-MIL-6 flight configurations.

5. Fins 1, 3, 5, and 1* have steel base structures and Fins 2, 4, 6, and 3* have aluminum base structures.

II. TEST CONFIGURATIONS, RATIONALE, AND DATA

A. Large First Generation Pneumatic Actuator on Missile Actuator Section

The test setup shown in Figure 1 was as close to MIL Flight No. 6 as possible. Figure 2 defines the axes and the two accelerometer positions utilized. The very small accelerometer was not large enough to influence the mode frequencies to be measured. In each configuration, the accelerometer response in the vertical ($\bar{z}$) and transverse ($\bar{x}$) directions are measured when the fin is given a disturbance in the measured direction, sometimes referred to as the twang test.

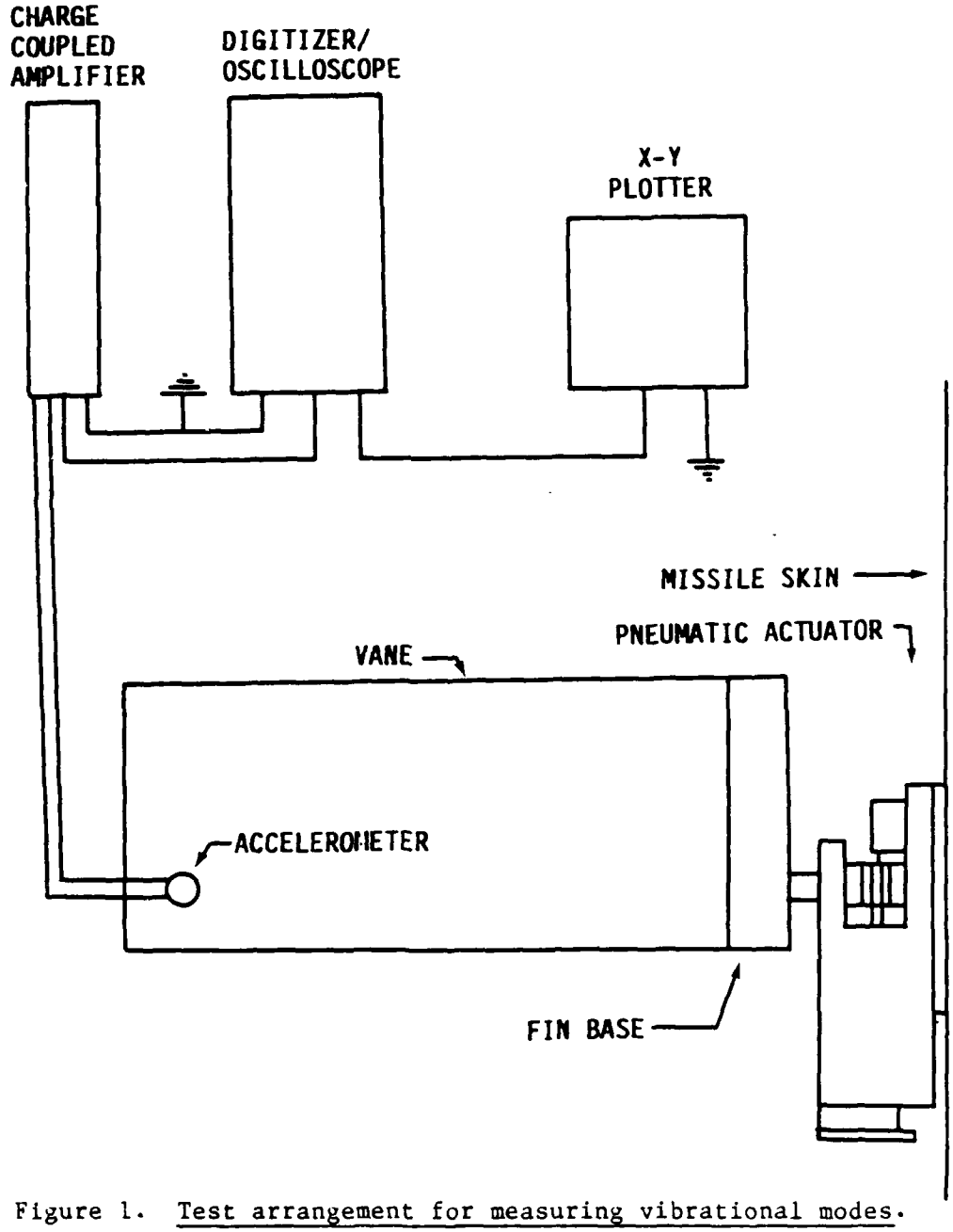

Figure 1. Test arrangement for measuring vibrational modes.

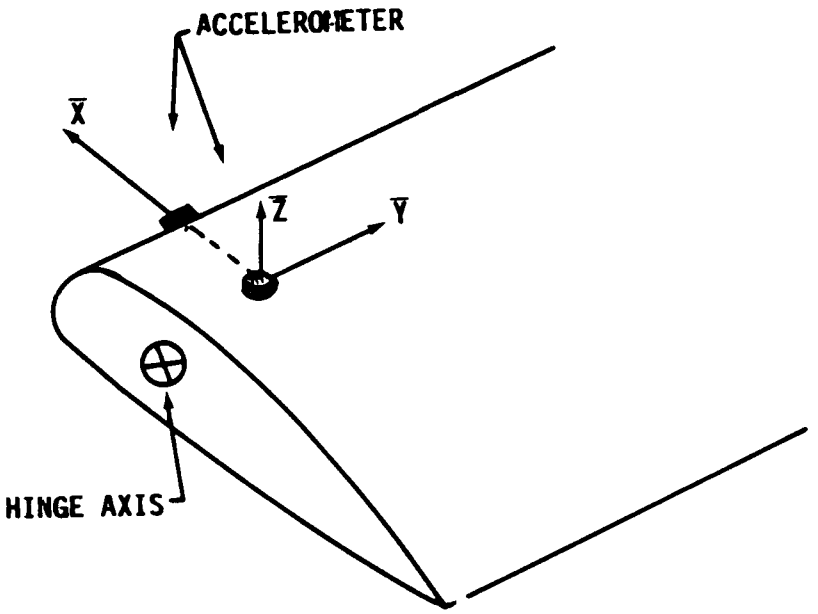

Figure 2. Sketch of the control fin, the two accelerometer positions, and the associated sensitive axes x and z.

The first test was conducted without shim stock material in the shaft/ fin-base to take out the loose motion in this joint. Figures 3, 4, and 5 show this data. Notice that the primary mode frequency in both directions is about 50 Hz. The activation of the pneumatic servo did not change this frequency but the remainder of all data is with the servo activated. Figure 6 was recorded with a very soft disturbance which excited a 160 Hz mode. Figure 7 was recorded with a similar soft disturbance that excited the basic 80 Hz mode but eventually settled out to the 160 Hz secondary mode. These are due to the fin spring vibrations; the modulation (Figure 6) is due to energy exchange between the planes of the vibration. The modulation frequency is, of course, not repeatable and depends on the disturbance.

The annotations in the upper right-hand corner of Figures 3 through 21 are the unit time scale and Δ is the time between the cursors. The annotations at the bottom of the figures are the vertical voltage scale factor, Δ gives the voltage between cursors, and $1/\Delta T$ gives the inverse of time-between-cursors.

Subsequently, the shim stock material was placed in the fin/shaft joint, as it was in MIL No. 6, to take out the small amount of loose motion. The results are shown in Figures 8, 9, and 10. The primary transverse ($\bar{x}$) mode frequency increased slightly because the shim material was in the $\bar{y}$-$\bar{z}$ plane and tightened the joint for $\bar{x}$ type motion. The shim was essentially absent in the $\bar{x}$-$\bar{y}$ plane so as not to obstruct the shaft pin hole. The effect of the soft shim material in the vertical ($\bar{y}$-$\bar{z}$) plane was to act as a snubber, reducing the frequency to 42 to 48 Hz, depending to some extent on the vibrational amplitude.

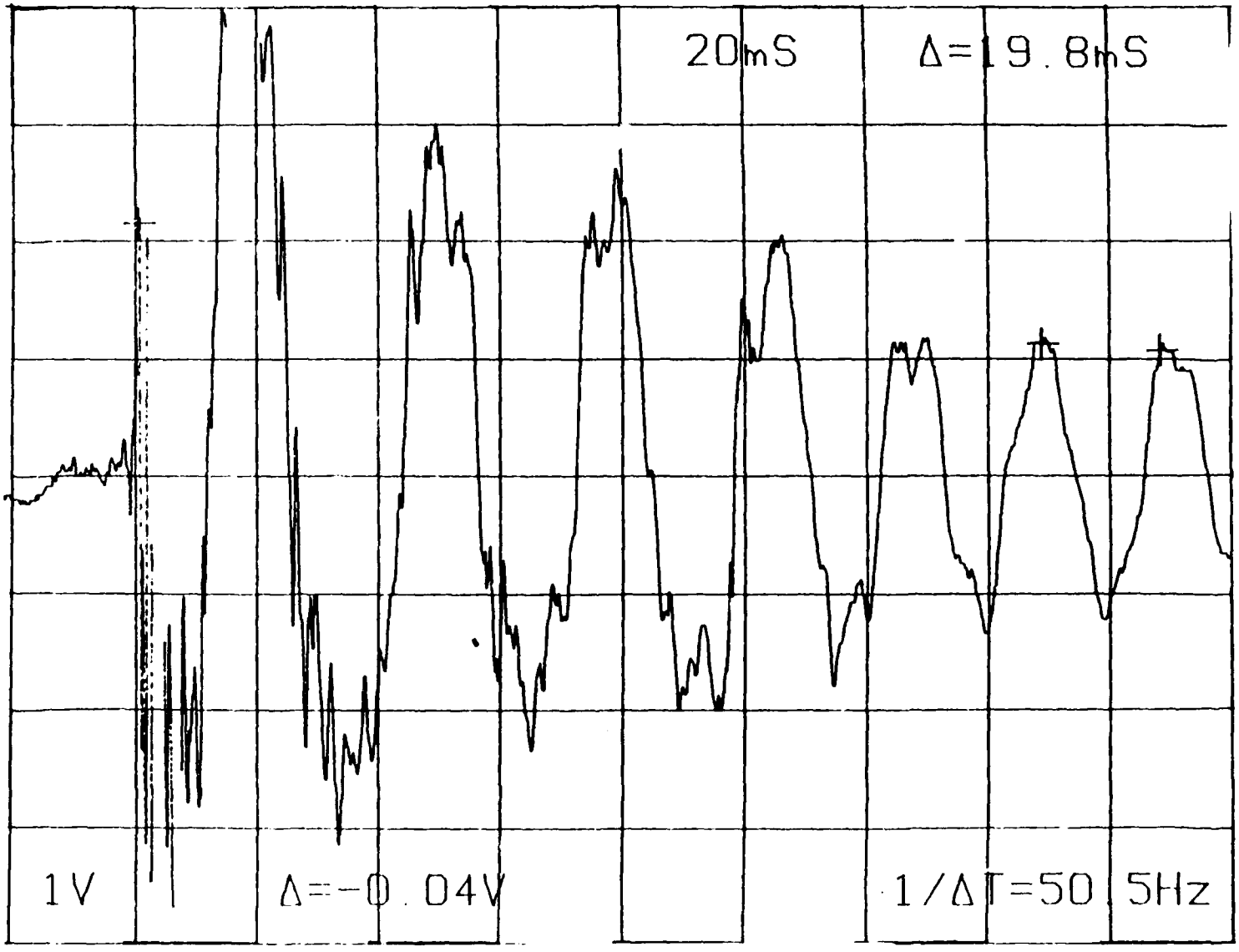

Figure 3. Vertical direction accelerometer signal (actuator not energized).

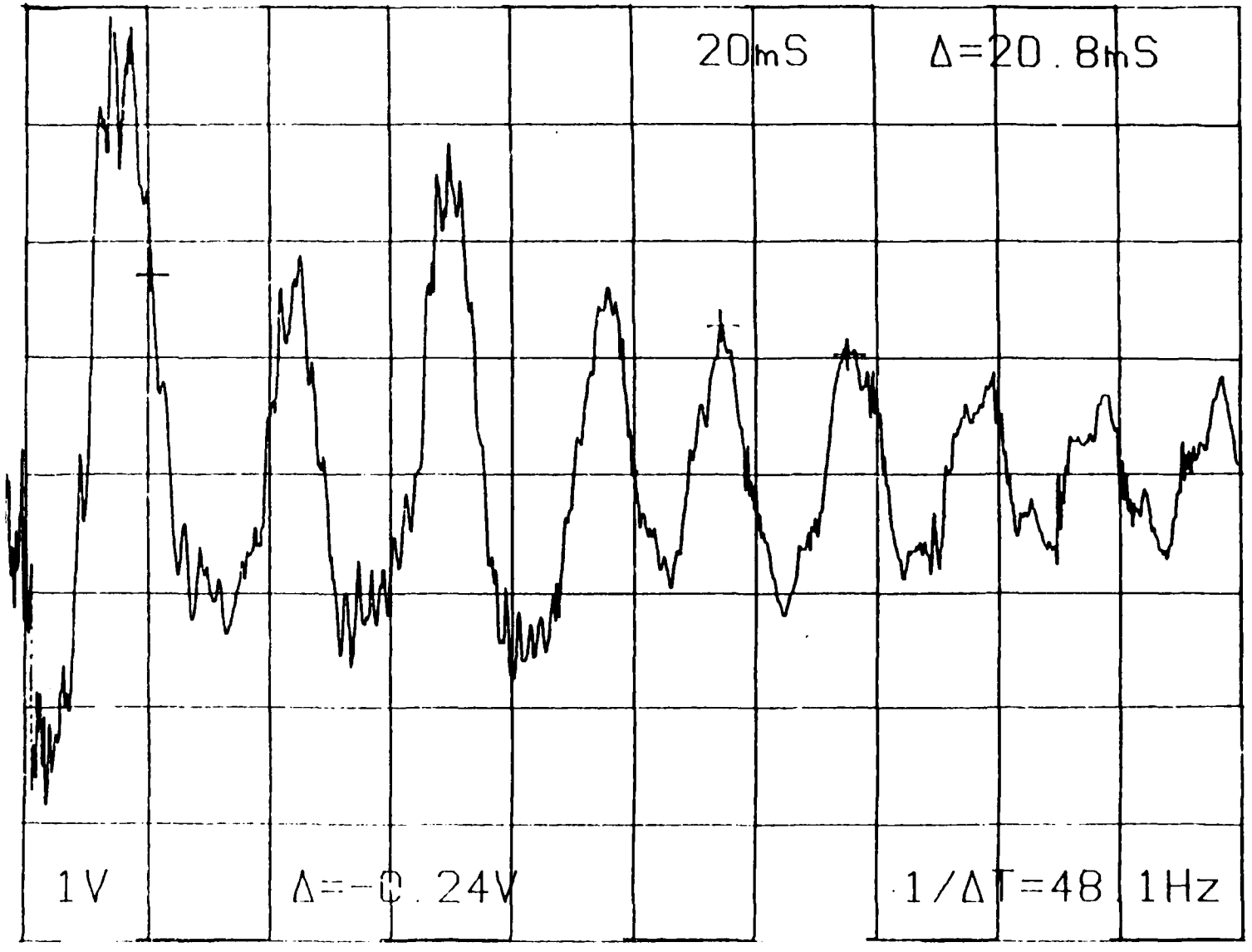

Figure 4. Vertical direction accelerometer signal (actuator energized).

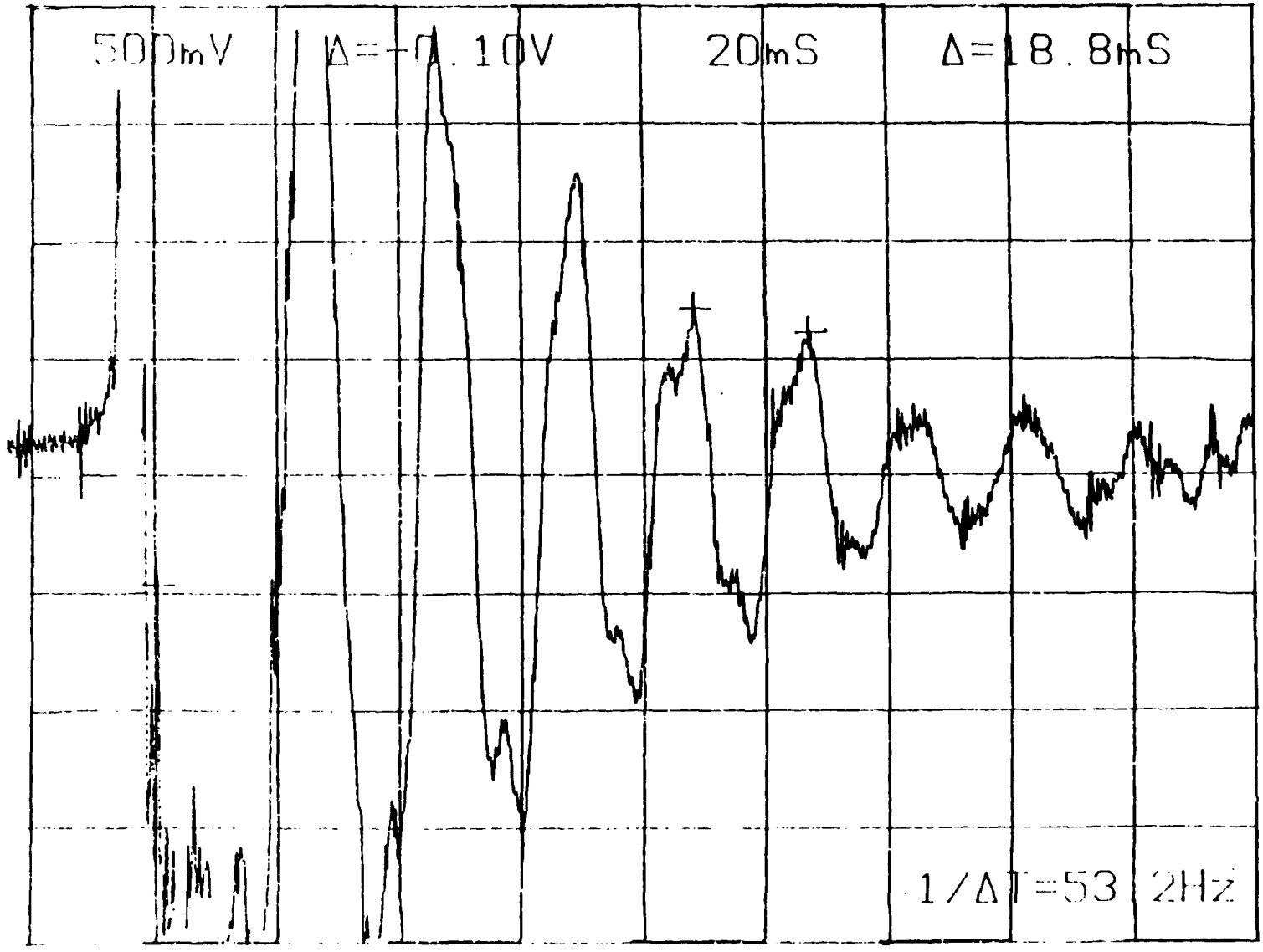

Figure 5. Transverse direction accelerometer signal.

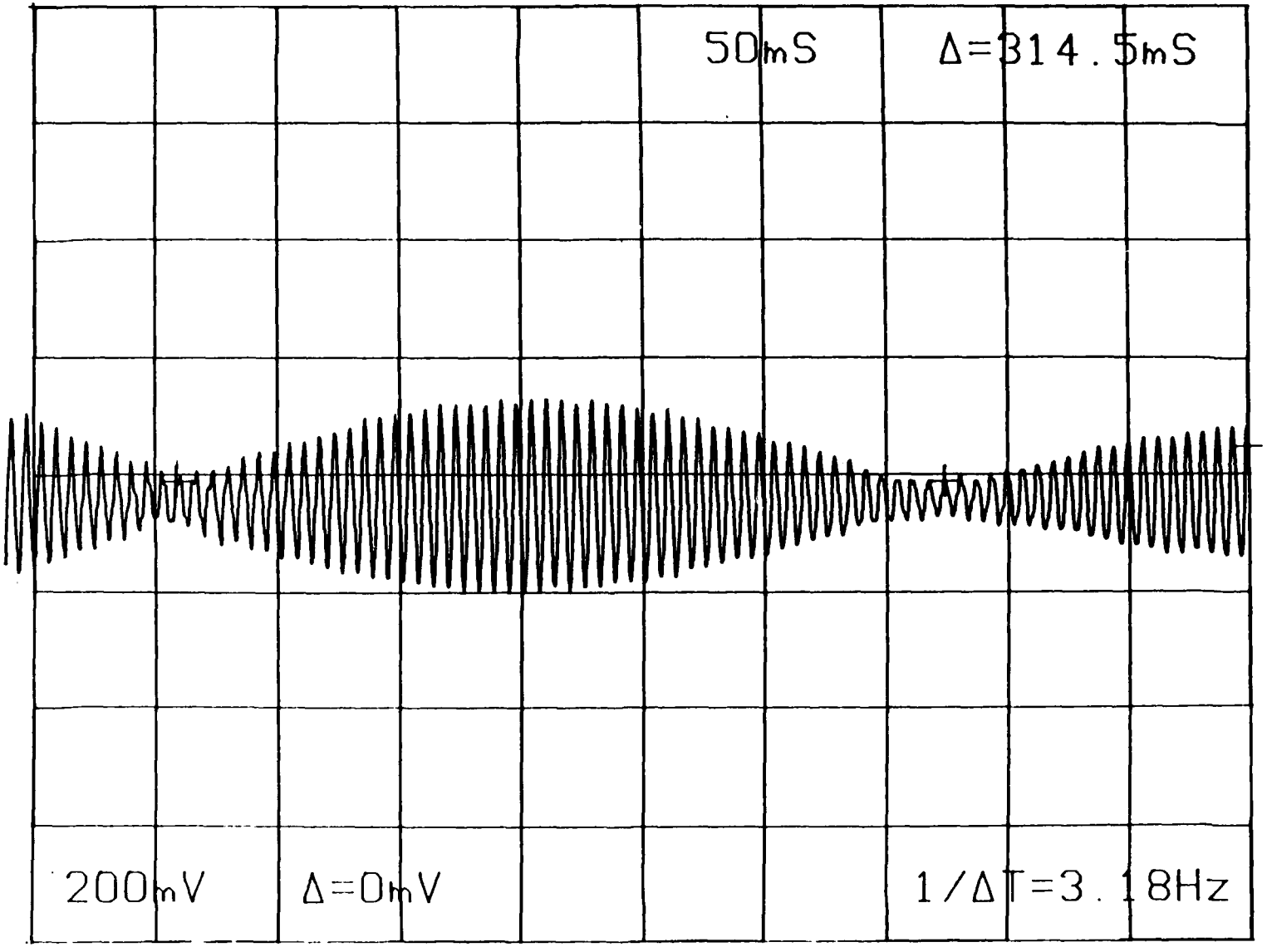

Figure 6. Vertical direction accelerometer signal (50 mS).

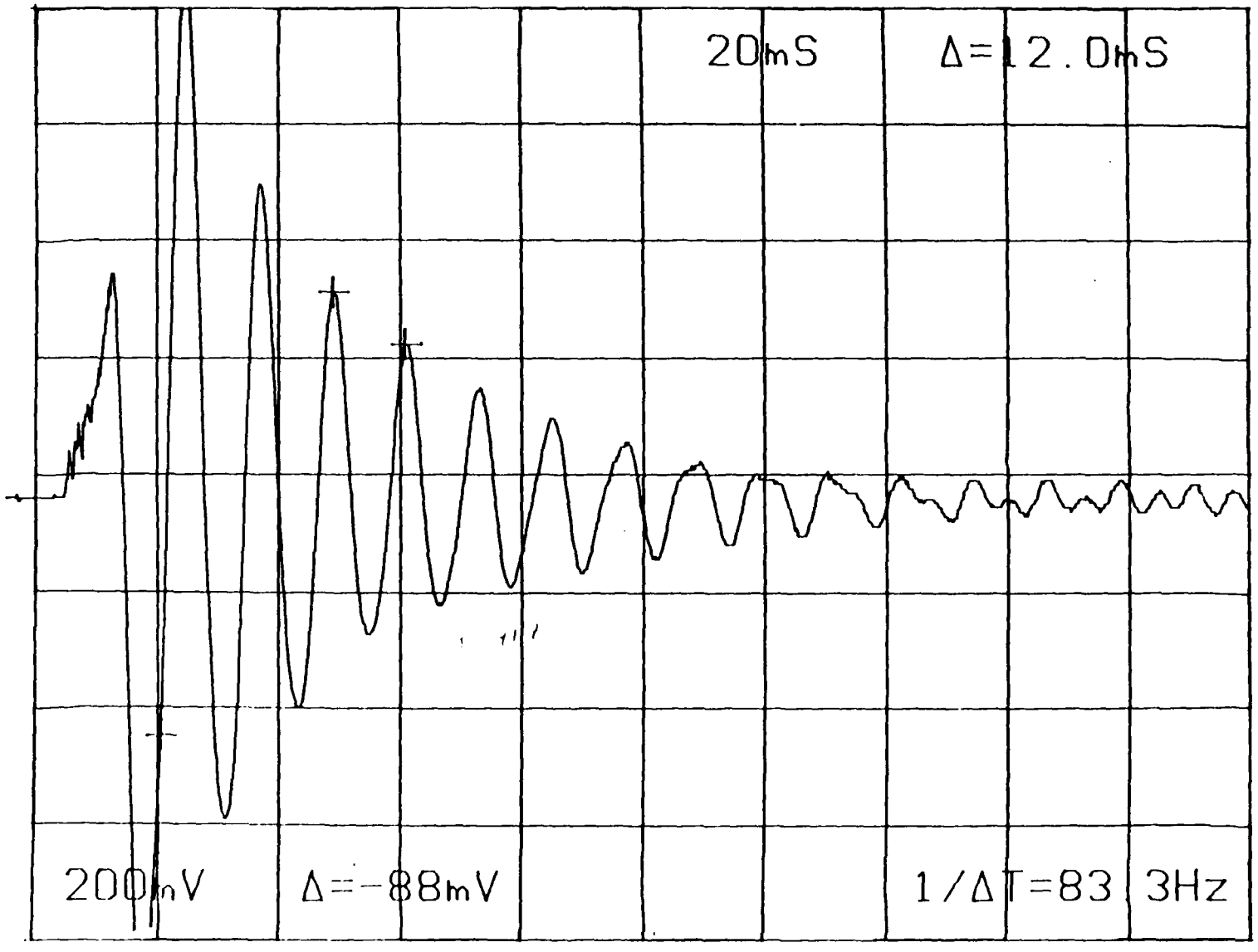

Figure 7. Vertical direction accelerometer signal (20 mS).

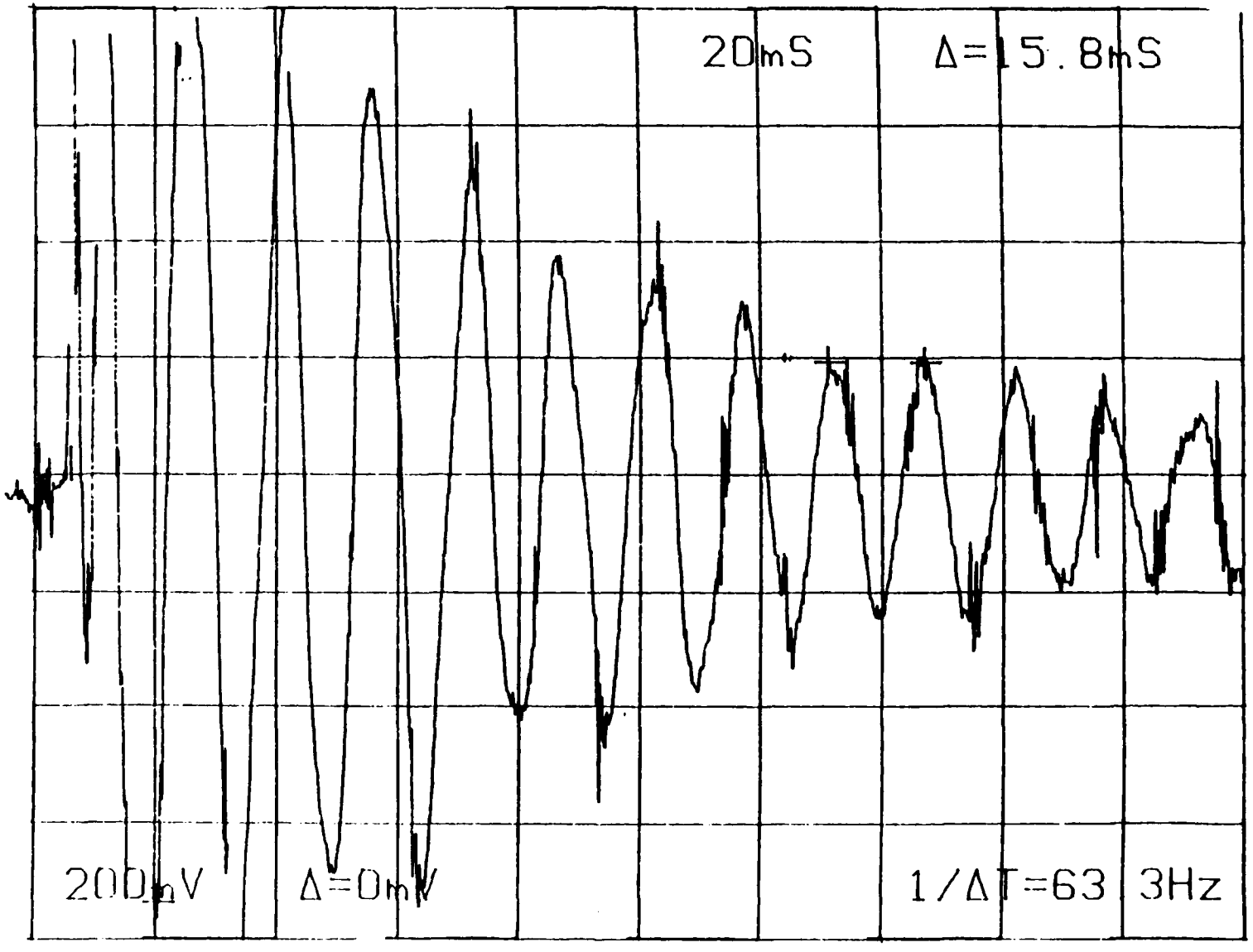

Figure 8. Transverse direction accelerometer signal with shim material placed in the shaft/fin-base joint.

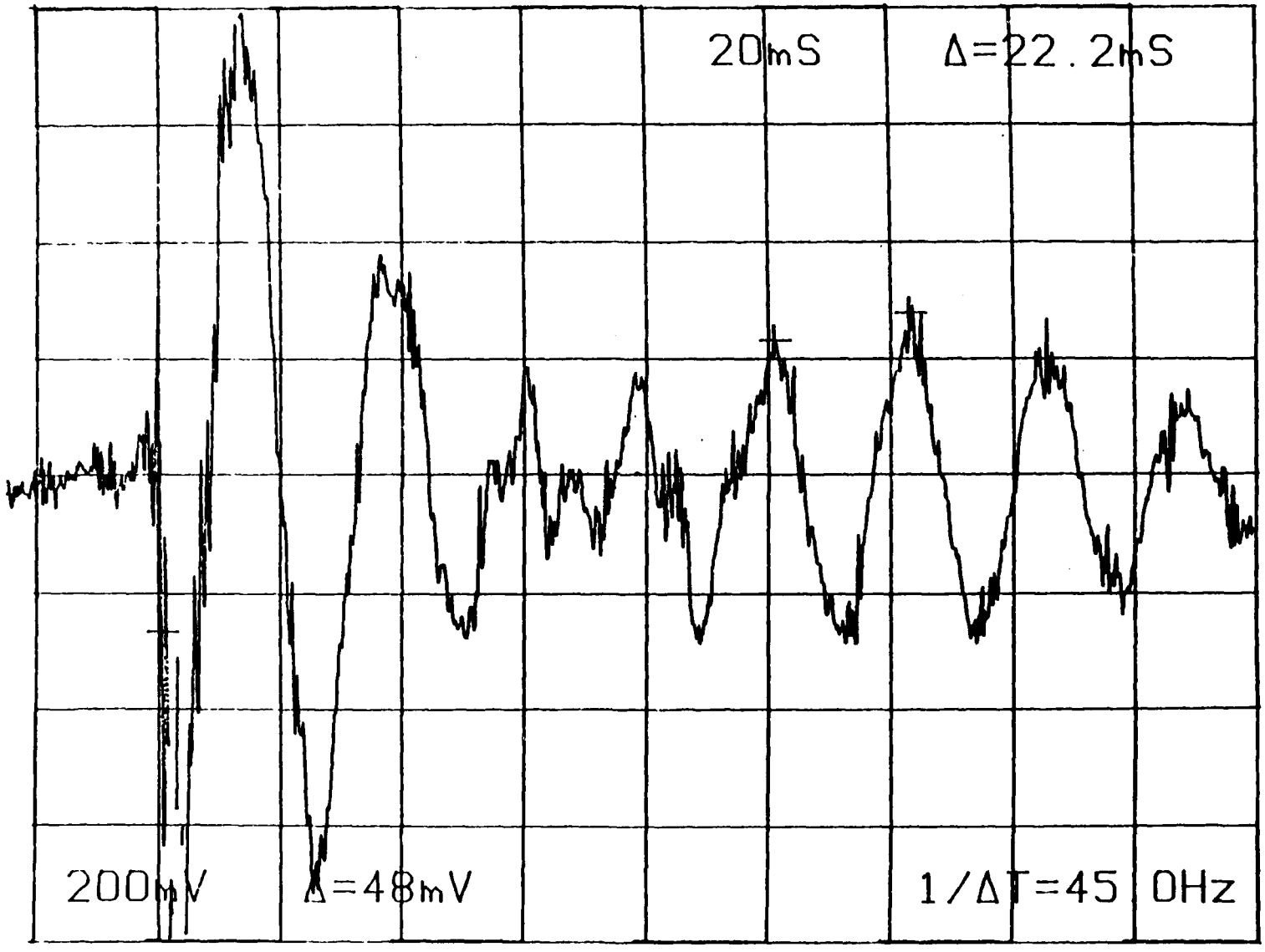

Figure 9. Vertical direction accelerometer signal with shim material placed in the shaft/fin-base joint.

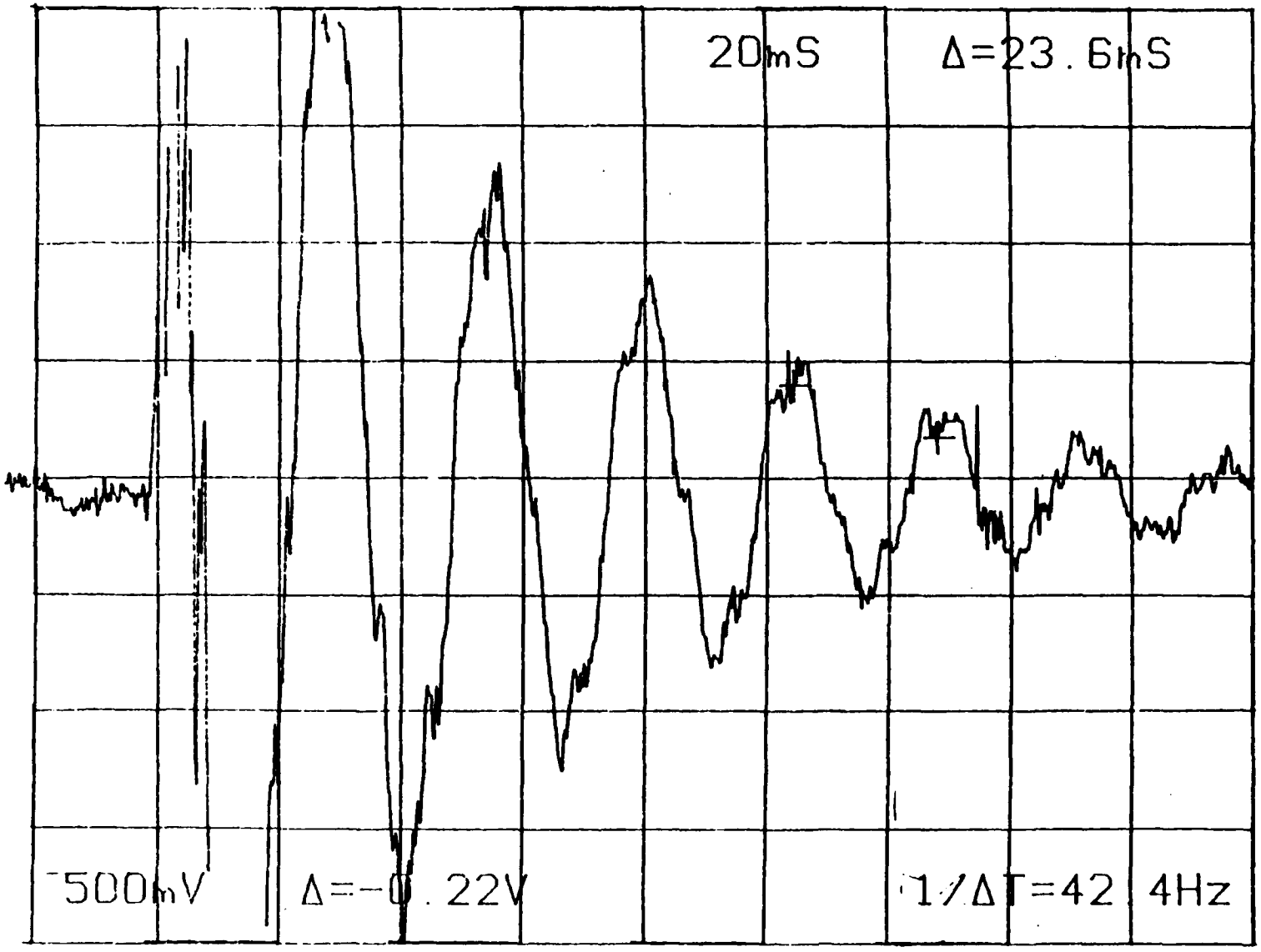

Figure 10. Transverse direction accelerometer signal with shim material placed in the shaft/fin-base joint.

B. Fin Base Fastened

The fin base structural member was securely fastened in a heavy vice to measure the mode frequencies of the fin itself which includes the fin locking mechanism. The results are shown in Figures 11, 12, and 13. The primary vertical frequency is about 80 Hz (Figure 11), whereas, the primary transverse mode frequency is about 328 Hz (Figure 12). Figure 13 was recorded with a different time scale to emphasize the modulation effect on the high frequency ($\bar{x}$) mode. The different modes of the spring (multiples of about 80 Hz) can be excited depending on the disturbance input.

C. Fin Shaft in Vice

To see if actuator bearing compliance has any impact on the 50 Hz mode, the fin was clamped in a heavy vice at 0.6 inches from the fin structure, corresponding to the distance to the first actuator bearing. The primary $\bar{z}$ mode was still close to 50 Hz (Figure 14). To see if the shaft length was the primary contributor to the 50 Hz mode, the vice clamp position relative to the fin structure was varied from 0.3 inches to 1.2 inches. The first and last of these positions are recorded in Figures 15 and 16. The frequency varied only between 55 and 47 Hz.

The above information on the impact of the shim material in the shaft/ fin interface joint, leads one to conclude that the shaft/fin joint itself is the source of the main 50 Hz (approximately) mode which shows up in both $\bar{z}$ and $\bar{x}$ directions. If this is true, it appears that the fin base structure around the fin shaft is the "spring" which defines this mode. As shown later, the fin structure itself is a contributor to this vibrational mode.

D. Aluminum Fin Structure, Unbalanced

Data were also recorded on the fin identified as No. 3* in Table 1. In addition, the actuator feedback potentiometer signal was recorded to check coupling into the rotational axis. Figure 17 records the accelerometer ($\bar{z}$ direction) and potentiometer signals for a $\bar{z}$ direction disturbance. The primary mode is about 54 Hz and there is no coupling into rotation about the hinge axis (the spikes on the pot signal are due to solenoid current transients coupled into the measurement circuits). Figure 18 records the same data as in Figure 17 but for a larger disturbance. Figure 19 records the $\bar{z}$ accelerometer and pot outputs when the fin is "deployed" from its folded position. The 31 Hz signal early in the transient is undoubtably influenced by the actuator servo response and, as will be demonstrated later, the highly damped fin-fold compliance term. Figure 20 records the event of a yet larger disturbance with still no coupling into roll about the hinge axis at the higher frequency.

E. Fin Deployment/Lock Spring Replaced by Steel Wire

The fin deployment/lock spring was replaced by a steel wire (much stiffer than the spring) and secured so that a very tight fit was obtained at the fin-fold joint. Figure 21 records the accelerometer output for a $\bar{z}$ disturbance. The 52 Hz primary mode is still present. There were 320 Hz and 800 Hz signals riding on the 52 Hz signal as well. Many other tests were conducted and no "modulation" type phenomena were noted.

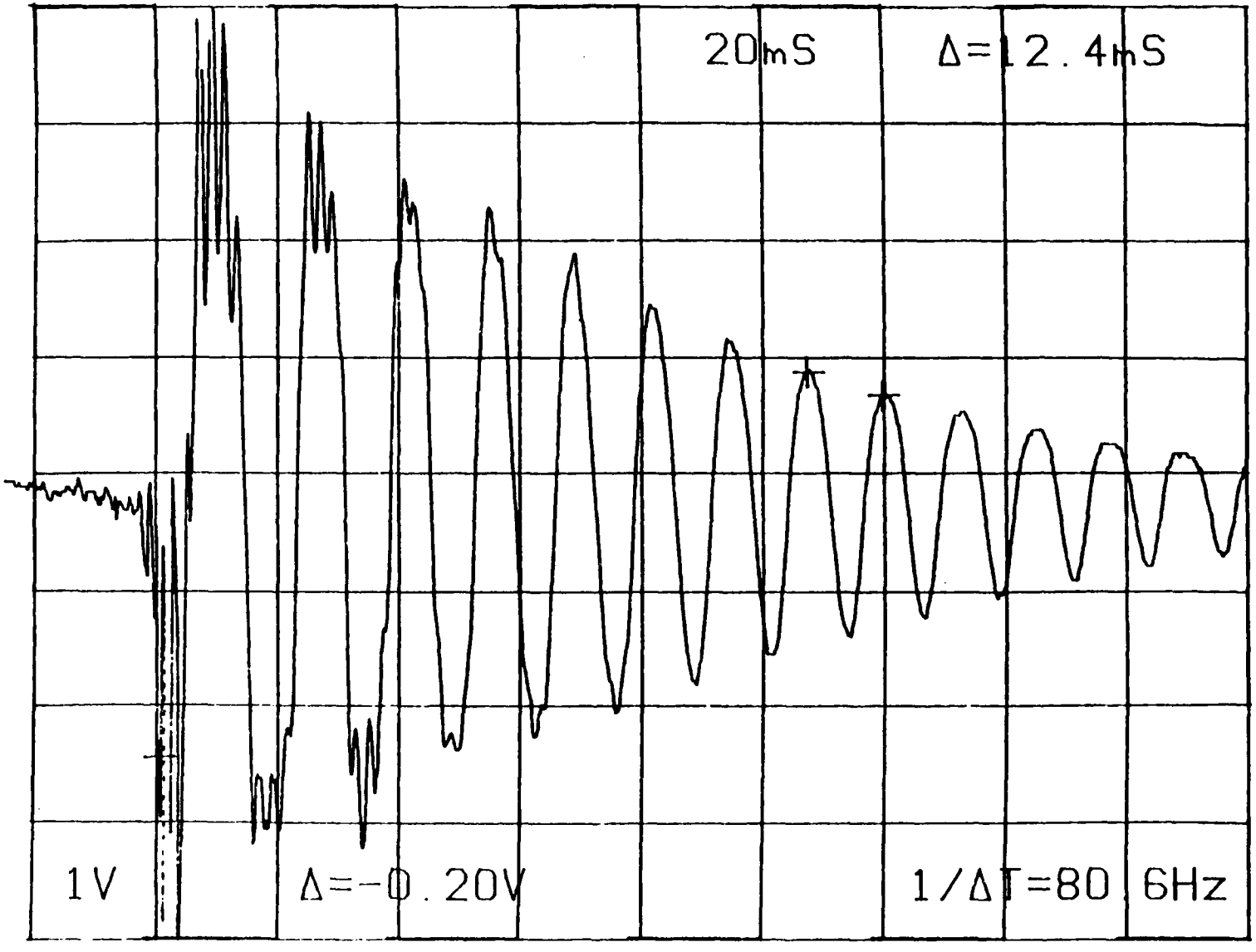

Figure 11. Vertical direction accelerometer signal with fin base clamp in heavy vice.

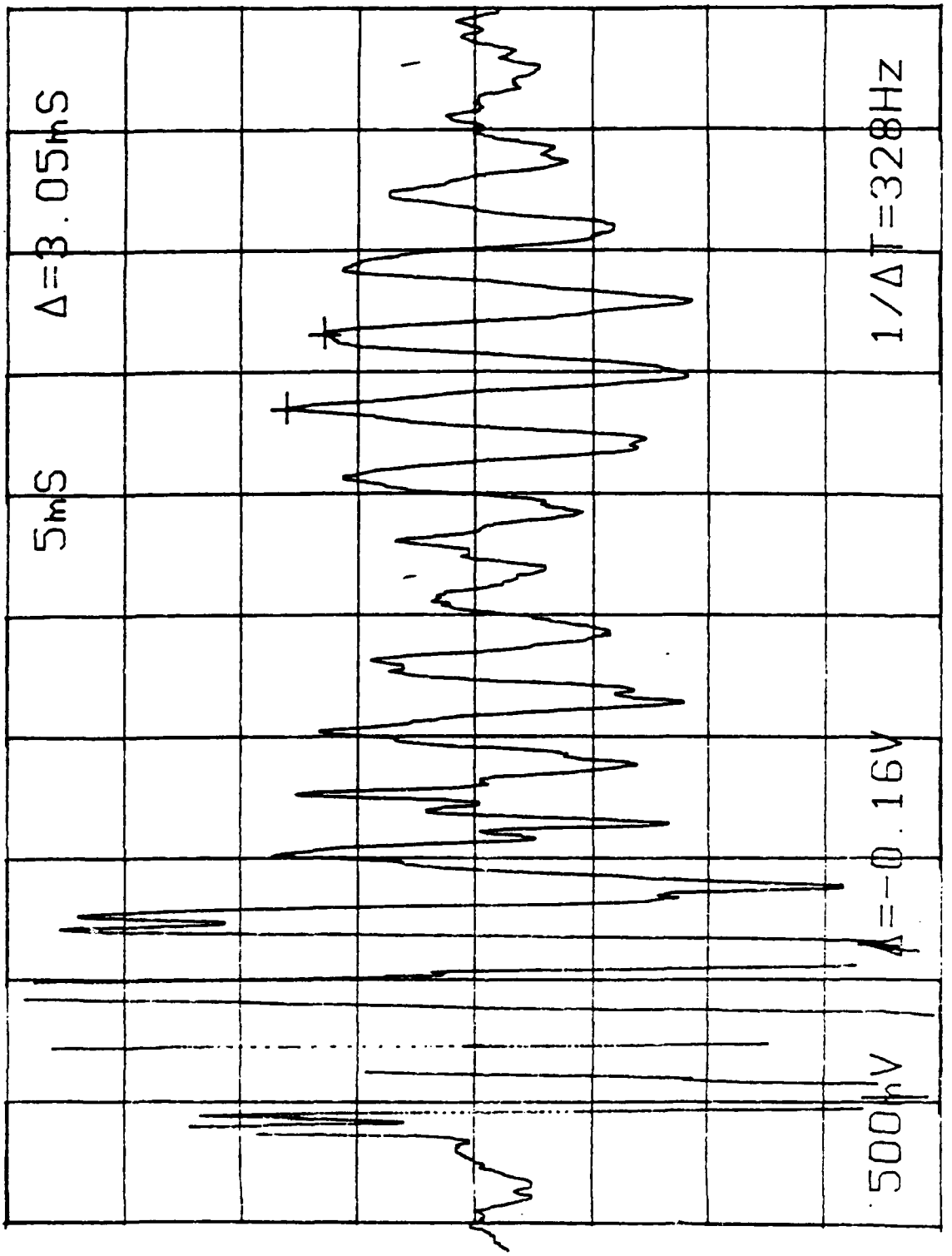

Figure 12. Transverse direction accelerometer signal with fin base clamped in heavy vice (5 mS).

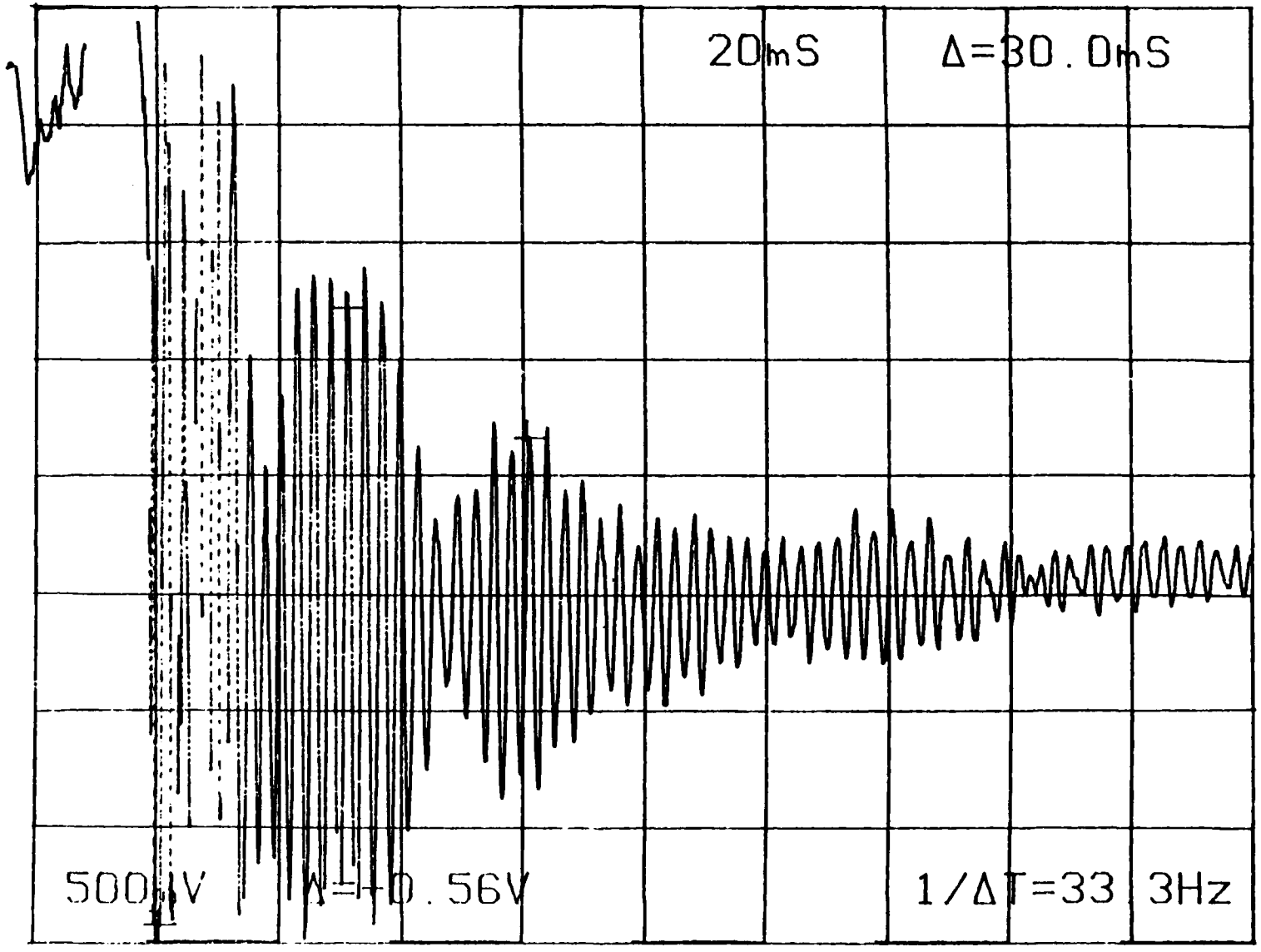

Figure 13. Transverse direction accelerometer signal with fin base clamped in heavy vice (20 mS).

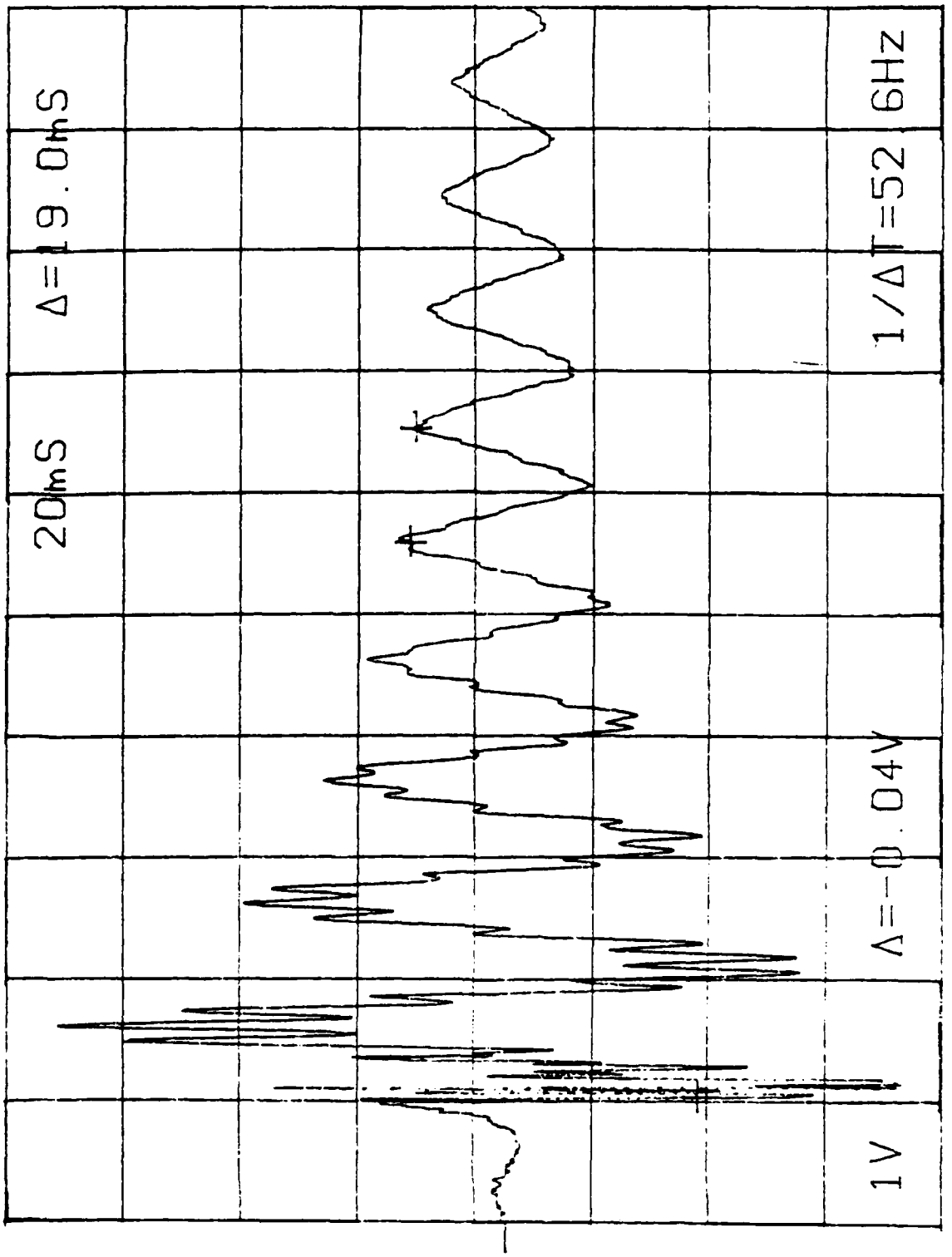

Figure 14. Vertical direction accelerometer signal, fin shaft clamped in vice (shaft length 0.6 in).

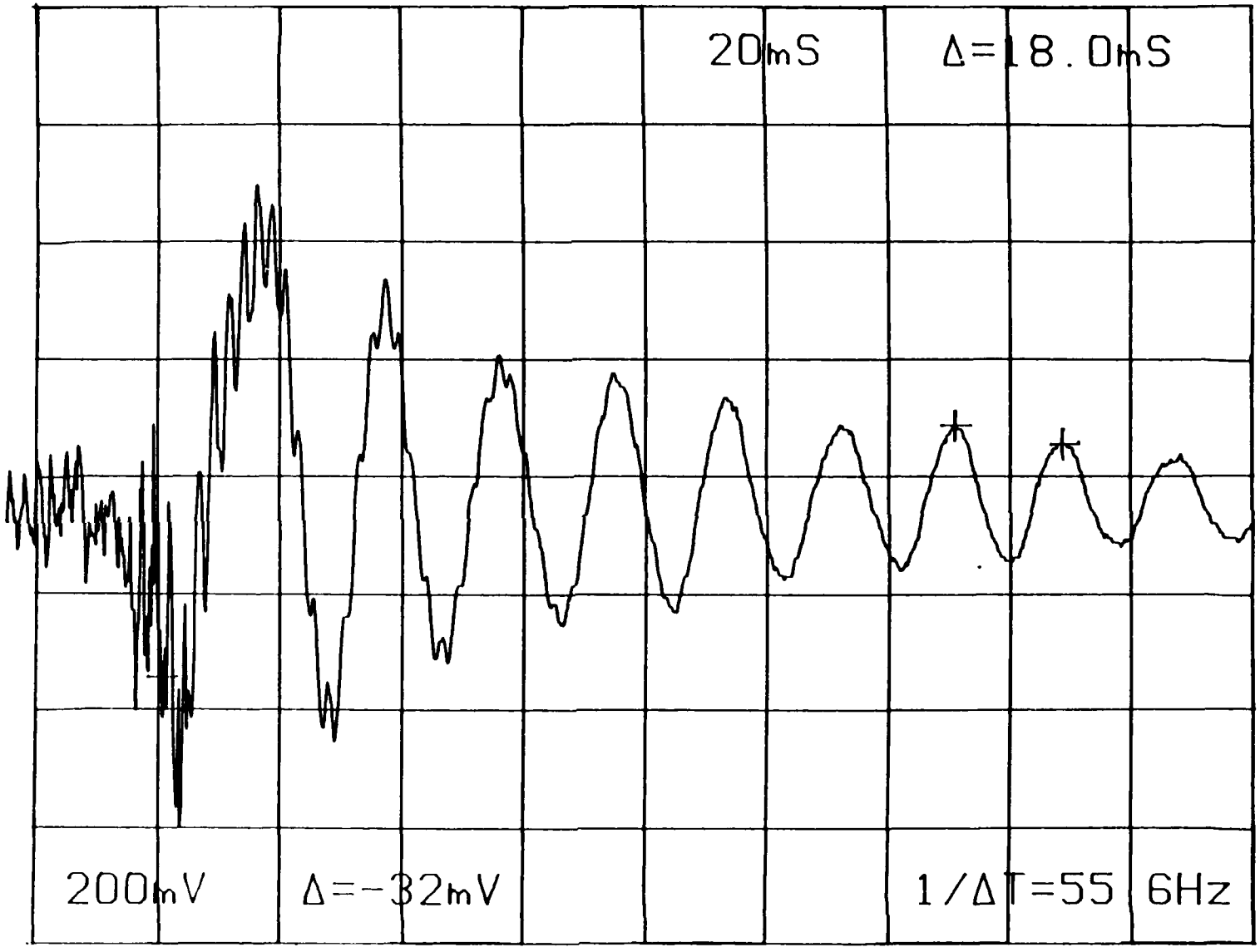

Figure 15. Vertical direction accelerometer signal, fin shaft clamped in vice (shaft length = 0.3 in).

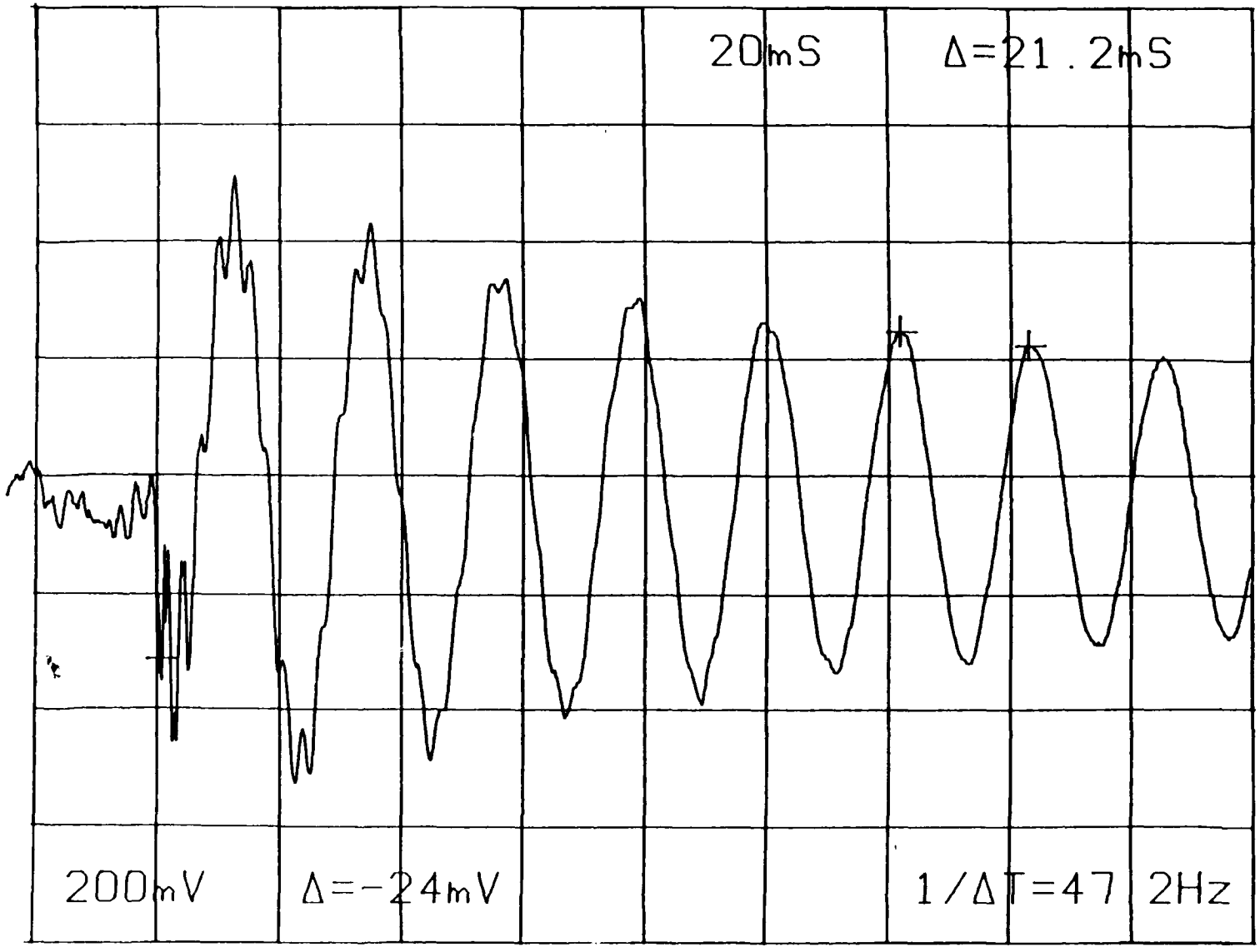

Figure 16. Vertical direction accelerometer signal fin shaft clamped in vice (shaft length = 1.2 in).

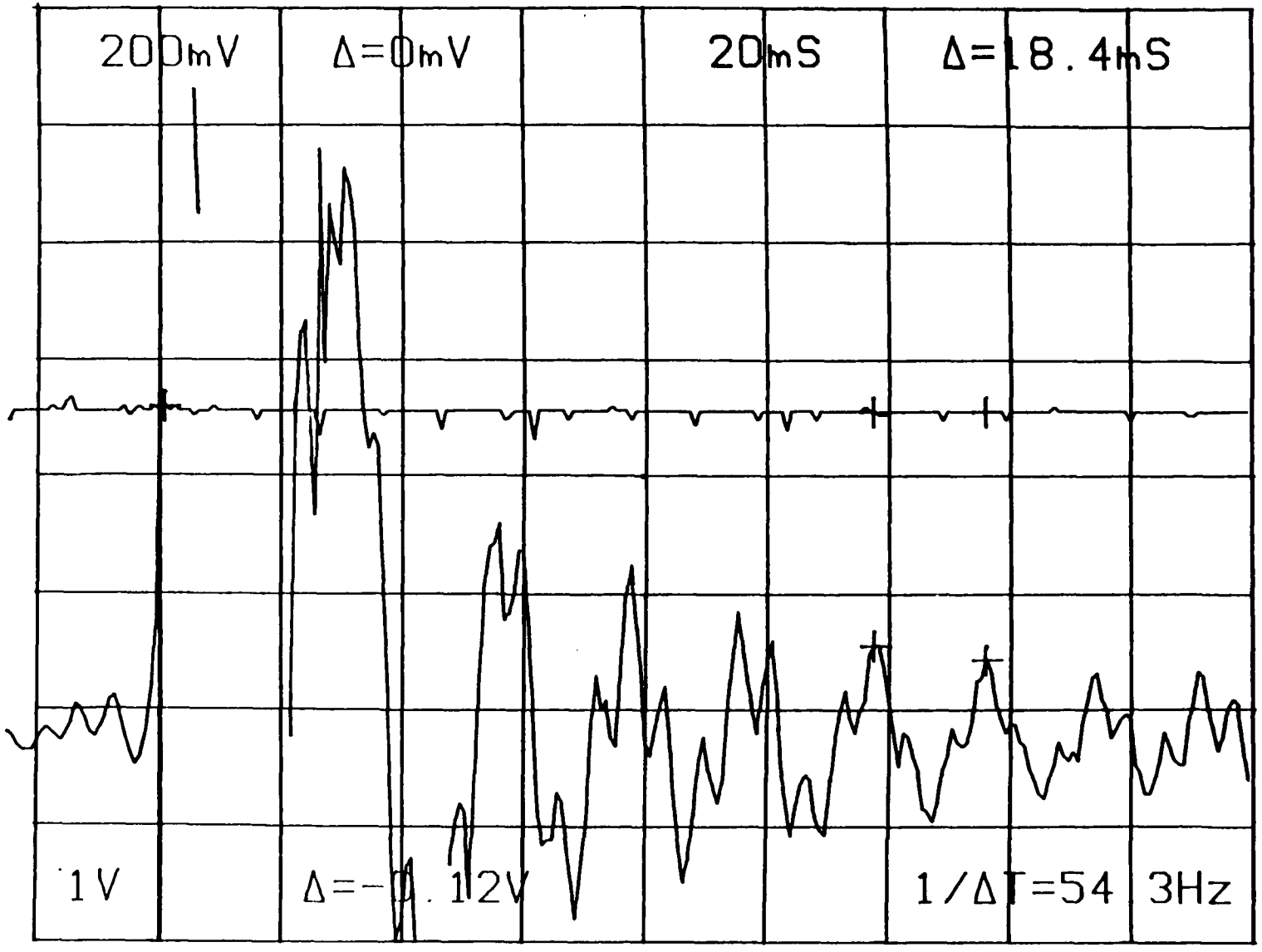

Figure 17. Vertical direction accelerometer and feedback potentiometer signals, normal actuator section mounting (aluminum base fin).

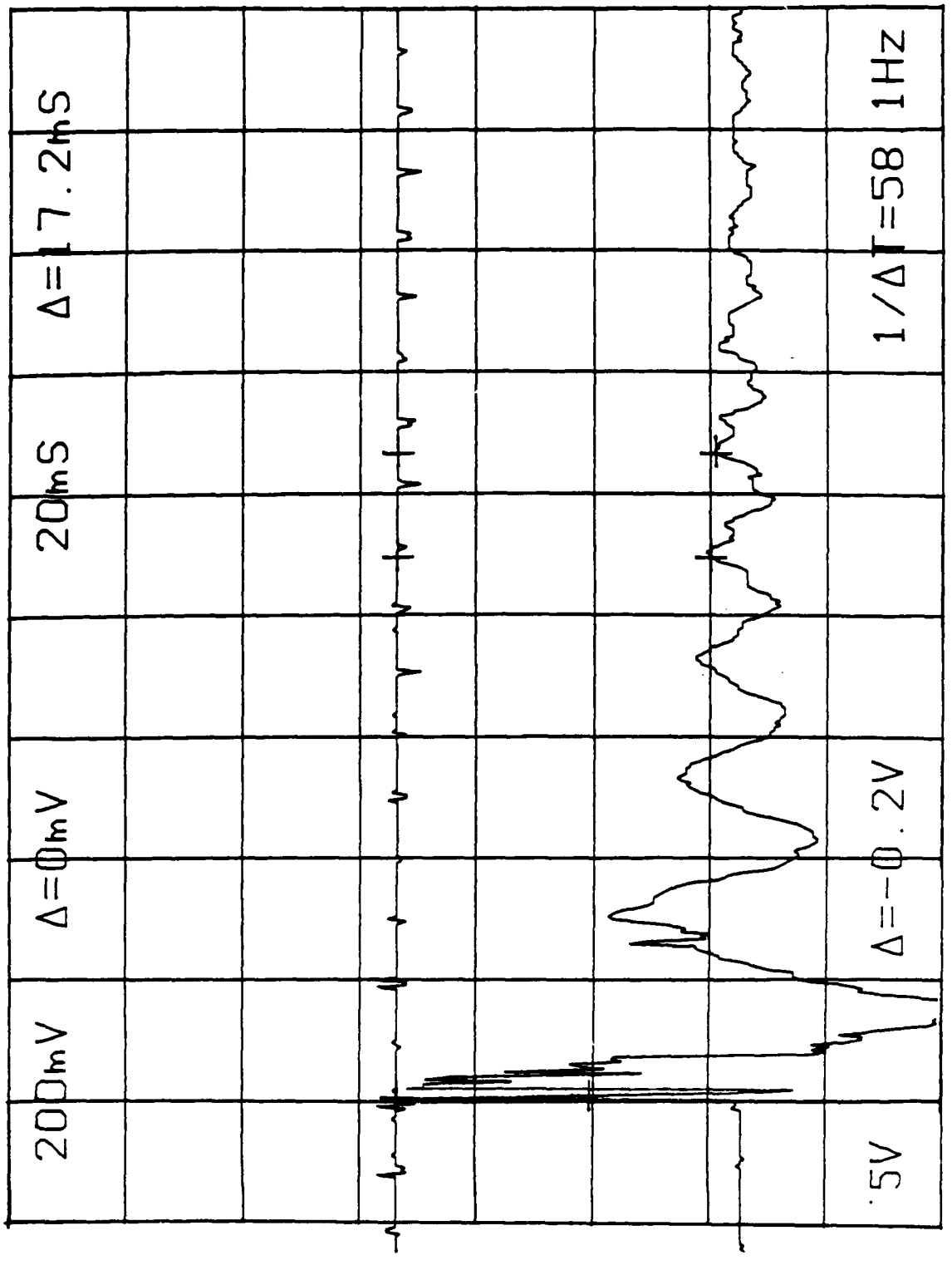

Figure 18. Vertical direction accelerometer and feedback potentiometer signals, normal actuator section mounting (aluminum base fin).

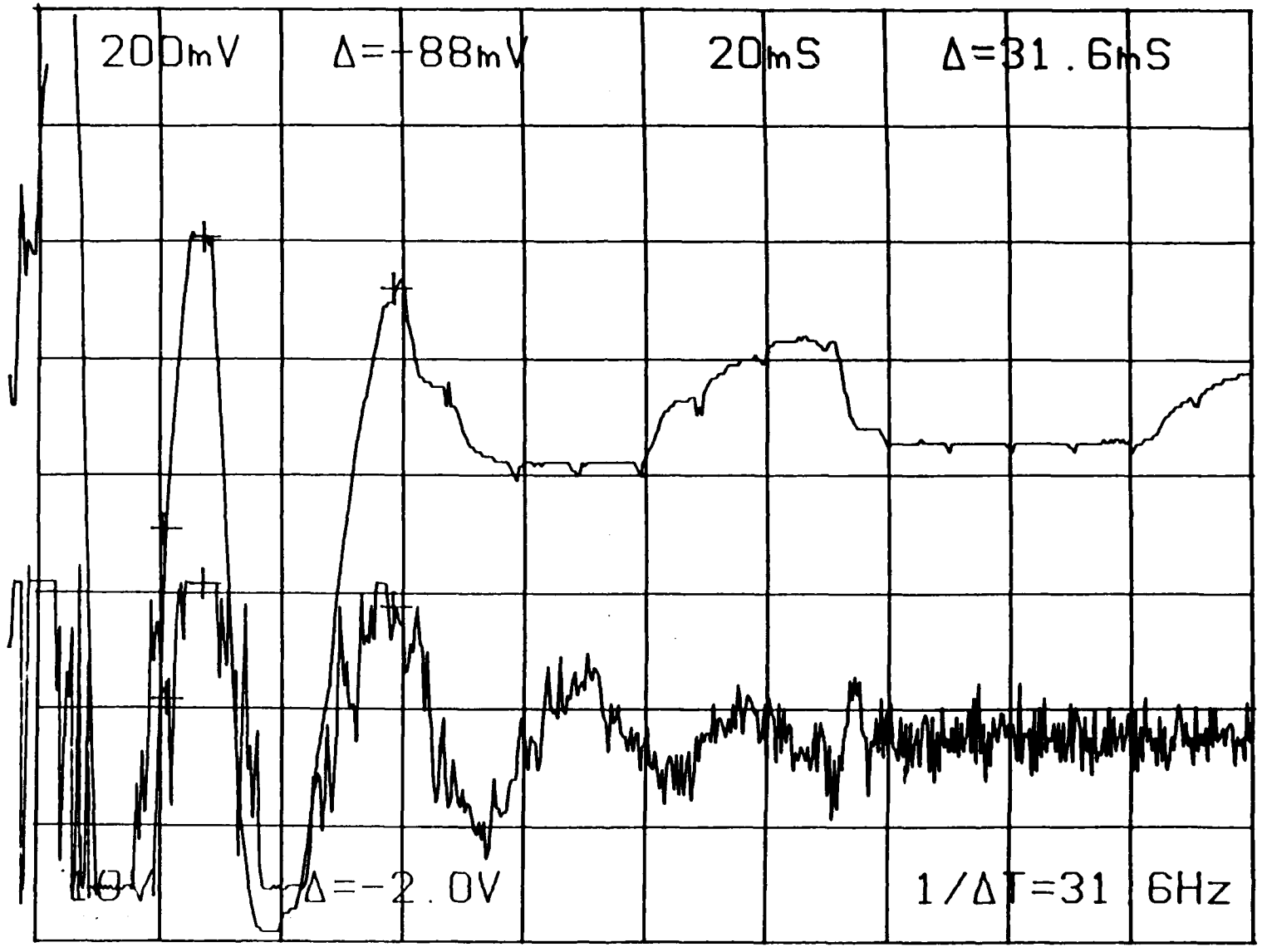

Figure 19. Vertical direction accelerometer and feedback potentiometer signals, fin deployed from a 45° folded position.

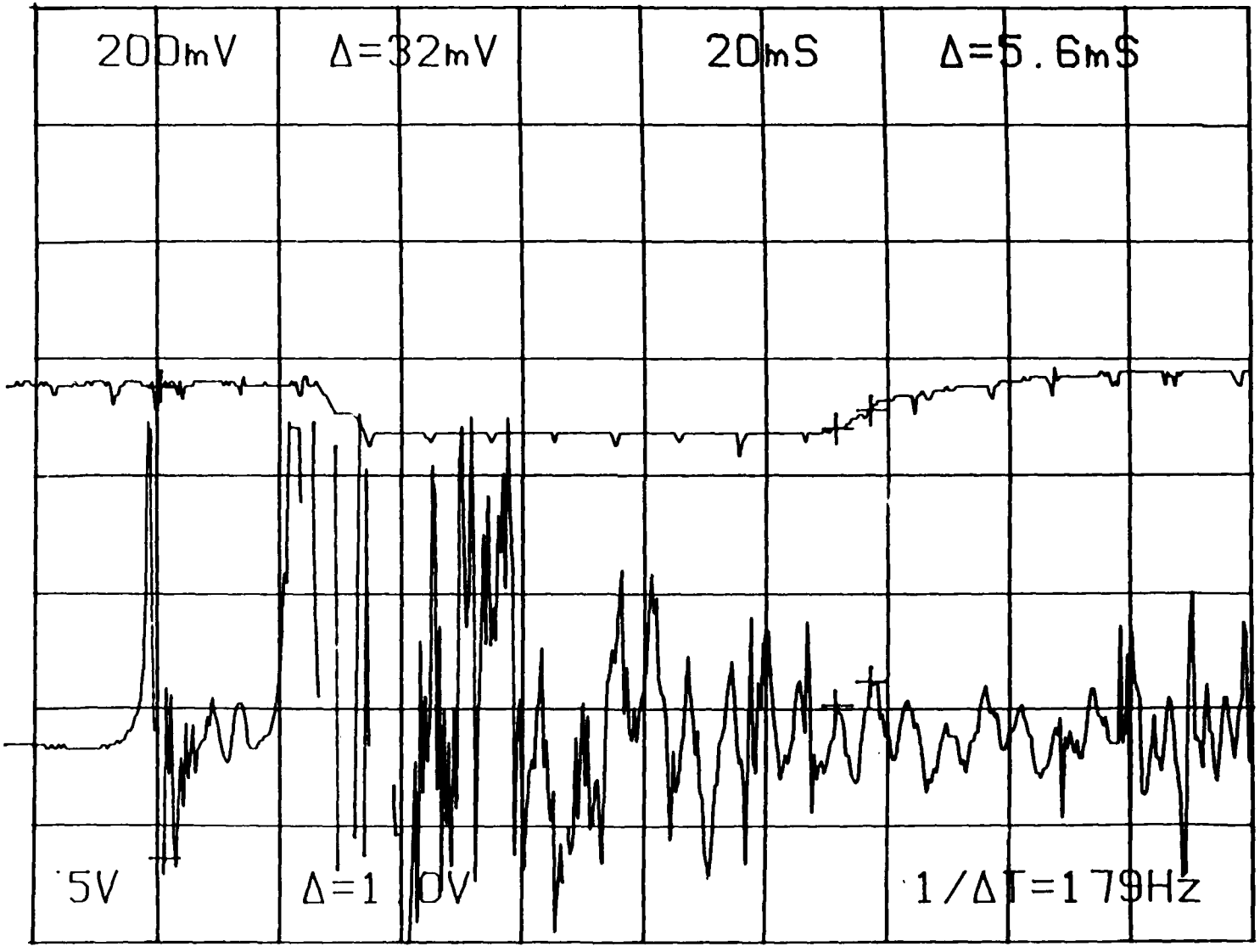

Figure 20. Vertical direction accelerometer and feedback potentiometer signals, fin deployed from a 45° folded position.

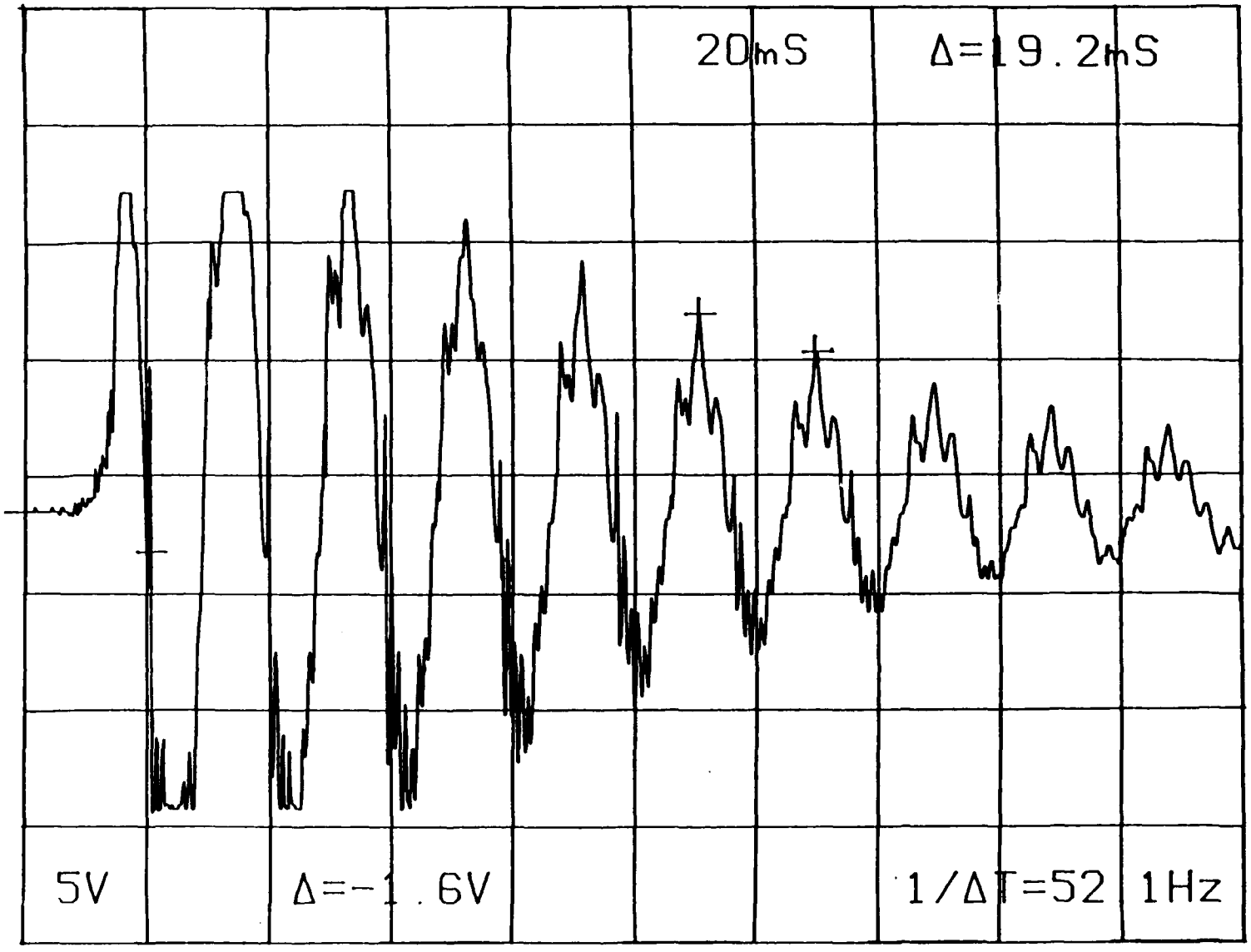

Figure 21. Vertical direction accelerometer signal, fin spring removed and replaced with steel wire, for a tight fit at fin-fold joint.

F. Fin, Fin Fold Mechanism, and Fin Shaft Spring Constants

One phenomenon that seemed to be confirmed during the previous step force release tests with accelerometer measurements was that the vibrational mode due to the fin-fold/fin-deployment mechanism couldn't be identified. However, comparatively large angular deflections were easily observable at this fin-fold joint when a moderate force was applied at the fin tip. It was speculated that the sliding motion at this joint provided enough damping so that a repetitive (countable) frequency was not observed in the accelerometer signal. This was intuitively demonstrated and the identity of the compliance terms that determine the 50 Hz mode were identified, albeit with some minor assumptions.

Tests were conducted where first, the fin base structure and then, the fin shaft were clamped in a vice and the fin-body/fin-fold mechanism stiffness measured (Figure 22). The force versus wing tip displacement ($\bar{z}$) for both test configurations are shown in Figure 23. The soft region around the nominal (zero) position, defined by slope K_3, is due to the fin-fold mechanism. Once all the loose motion in this mechanism is exceeded, the stiffness is dominated by the shaft/base structure ($\bar{K}_1$) or the shaft/base structure/fin

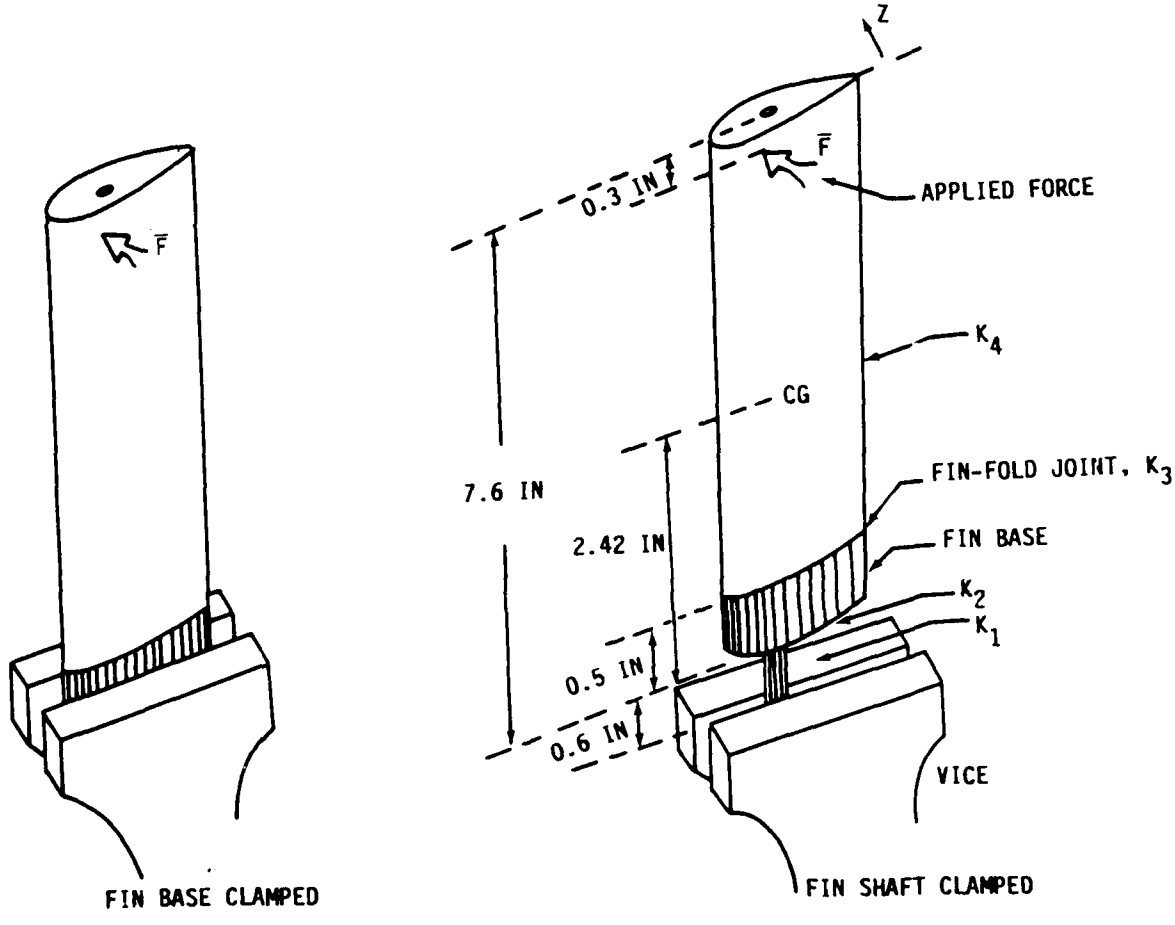

Figure 22. Fin capture arrangement for measuring fin stiffness terms.

structure (K_2). A simplified schematic of the stiffness is shown in Figure 24, where the mass is assumed lumped in "m." These particular spring rates (K_1 through K_4) are those effective spring rates when a force is applied at the wing tip (Figure 22). When the limits around K_3 are exceeded, its stiffness goes to "infinity."

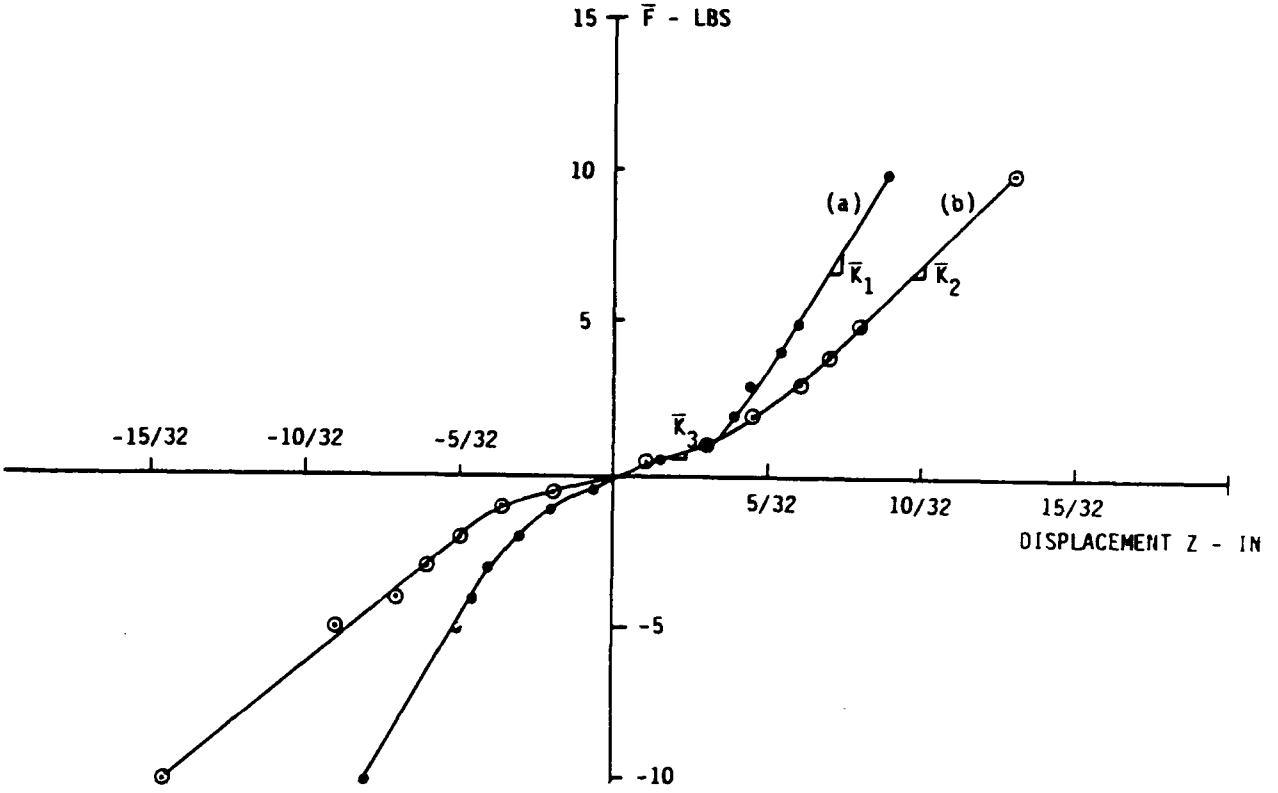

(a) Fin body and fin-fold structure only.

(b) Total fin body, fin-fold mechanism, fin base, and fin shaft.

Figure 23. Measured stiffness.

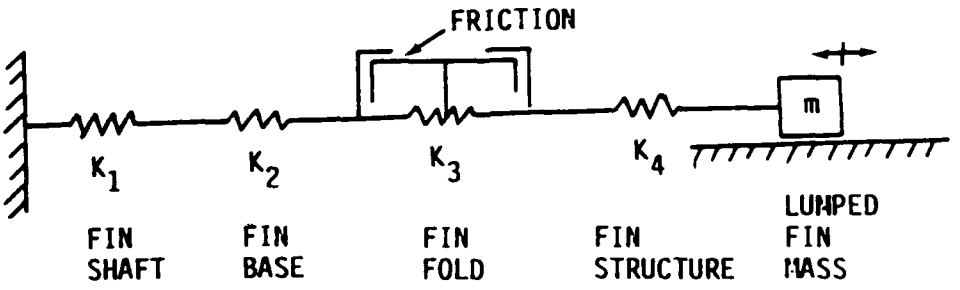

Figure 24. Schematic diagram of fin spring terms with lumped mass.

The springs K_1 through K_4 are related to the measured spring constants of Figure 23 by relations:

$$\bar{K}_1 = K_4 \quad . \tag{1}$$

$$\bar{K}_2 = \frac{K_1K_2K_4}{K_1K_2 + K_1K_4 + K_2K_4}$$

$$\approx \frac{K_2K_4}{K_2 + K_4} \quad . \tag{2}$$

$$\bar{K}_3 = \frac{K_1K_2K_3K_4}{K_1K_2K_3 + K_1K_2K_4 + K_1K_3K_4 + K_2K_3K_4} \tag{3}$$

$$\approx K_3 \quad .$$

The values of $\bar{K}_1$, $\bar{K}_2$, and $\bar{K}_3$ are determined from Figure 21 to be

$$\bar{K}_1 = 53.4 \text{ lb/in.} \tag{4}$$

$$\bar{K}_2 = 32 \text{ lb/in.} \tag{5}$$

$$\bar{K}_3 = 12 \text{ lb/in.} \tag{6}$$

Let the shaft/base structural spring be defined by

$$\bar{K}_4 = \frac{K_1K_2}{K_1 + K_2} \quad , \tag{7}$$

and the fin-fold/fin spring defined by

$$\bar{K}_5 = \frac{K_3K_4}{K_3 + K_4} \quad . \tag{8}$$

When spring K_3 is "bottomed-out" or limits (Figure 21, Curve (a))

$$\bar{K}_5 = K_4 = \bar{K}_1 \tag{9}$$

and (Figure 21, Curve (b))

$$\frac{\bar{K}_4\bar{K}_5}{\bar{K}_4 + \bar{K}_5} = K_2 \quad . \tag{10}$$

Thus,

$$\frac{1}{\bar{K}_4} = \frac{1}{\bar{K}_2} - \frac{1}{\bar{K}_1} = \frac{1}{32} - \frac{1}{53.4} \tag{11}$$

and

$$\overline{K}_4 \text{ (shaft/Base)} = 80 \text{ lb/in.} \tag{12}$$

The shaft spring K_1 may be accurately calculated (Figure 25) by the relation

$$\delta = \frac{PL^3}{3EI} \quad , \tag{13}$$

where

$$I = \frac{\pi r^4}{4} = 1.917 \times 10^{-4} \quad , \tag{14}$$

and

$$E = 30 \times 10^6 \text{ lb/in.} \tag{15}$$

Thus,

$$\tilde{K}_1 = \frac{P}{\tilde{\delta}} = 79{,}875 \text{ lb/in.} \tag{16}$$

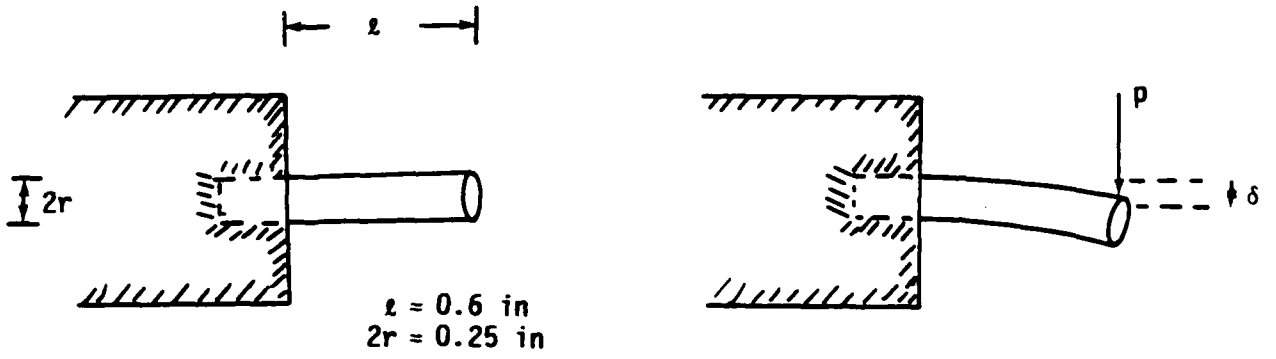

(a) AT REST

(b) DEFLECTION DUE TO FORCE P

Figure 25. Fin shaft with side load.

The deflection $\tilde{\delta}$ may be translated out to 0.3 in from the wing tip where our measurements were made (Figure 26) by the relation:

$$\frac{\tilde{\delta}}{0.6} = \frac{\delta}{7.3 \text{ in} + 0.6 \text{ in}} \tag{17}$$

or

$$K_1 = \frac{P}{\delta} = \frac{0.6P}{7.9\tilde{\delta}} = \frac{0.6}{7.9} \quad (79{,}875) \tag{18}$$

$$= 6{,}066 \text{ lb/in.}$$

By comparing equations (12) and (18), it is obvious that the fin shaft is negligible in computing $\overline{K}_4$ (fin/base), i.e., the base stiffness is much less than the shaft stiffness. This corresponds to the deduction made earlier from the accelerometer measurements when the fin shaft length was varied:

$$\overline{K}_4 \approx K_2 \quad . \tag{19}$$

Now calculate the natural frequency, if only the fin base was the spring contributor. Assume that the fin mass is lumped at the CG. For this particular fin the CG is located 2.42 in. from the fin base and the weight is 0.357 lb. The effective spring (K_2 translated to the CG) is

$$\hat{K}_2 = \frac{7.6 \text{ in}}{2.42 \text{ in}} (80 \text{ lb/in}) = 251 \text{ lb/in.} \tag{20}$$

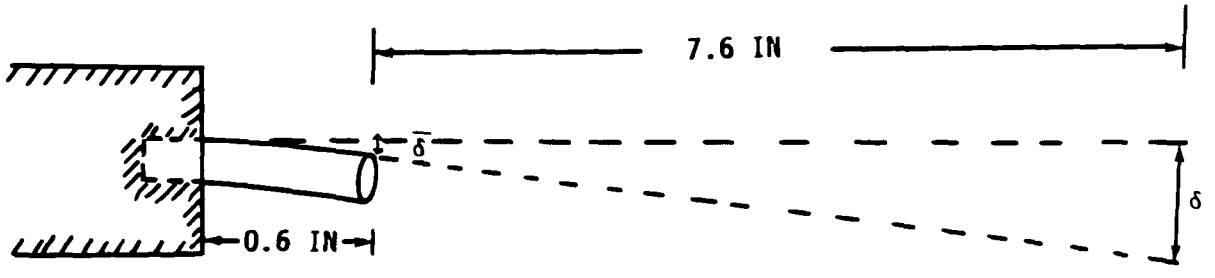

Figure 26. Wing tip deflection δ which translates to shaft tip deflection δ.

The natural frequency would be

$$f_{n1} = \frac{1}{2\pi}\sqrt{\frac{\hat{K}_2}{w/g}} = \frac{1}{2\pi}\sqrt{\frac{251}{0.357/386}} = 83 \text{ Hz.} \qquad (21)$$

Obviously the nominal 50 Hz (47 to 53 Hz) frequency noted earlier is not due just to the fin base.

Next, the natural frequency is calculated using the measured total spring $\bar{K}_2$ (assuming the fin-fold spring is inoperative). The measured $\bar{K}_2$ is translated from the wing tip to the CG by assuming that the total spring is a lumped element. This of course is not true, since the fin structure part of the spring is distributed along the wing. This is done, recognizing that the error and the fact that a technically exact analysis is not worth the effort required. The spring $\bar{K}_2$ translated to the CG is

$$\bar{K}_{2CG} = \frac{7.6-0.3}{2.42} \text{ (32 lb/in)} = 96.5 \text{ lb/in.} \qquad (22)$$

The natural frequency is

$$f_{n2} = \frac{1}{2\pi}\sqrt{\frac{96.5}{0.357/386}} = 51.4 \text{ Hz} \quad . \qquad (23)$$

Next, the natural frequency which would result strictly from the fin-fold joint is calculated. The spring $\bar{K}_3$ (Figure 23) is translated to the CG and the motion is assumed to take place at the joint. Referring to Figure 22 the effective spring at the CG is

$$\bar{K}_{3CG} = \frac{7.6-0.3}{2.42} \text{ (12 lb/in)} = 36.2 \text{ lb/in,} \qquad (24)$$

and the natural frequency is

$$f_{n3} = \frac{1}{2\pi}\sqrt{\frac{36.2}{0.357/386}} = 31.5 \text{ Hz.} \qquad (25)$$

A careful look at much of the accelerometer data in the z direction will show that the frequency is lower in the early part of the transient and that it settles out quickly to the 50 Hz mode. This is probably due to the fin-fold spring. The reason the oscillations do not settle down to the 31 Hz mode is that there is so much sliding friction in this close fit (fin-fold) joint that motion in this joint quickly dies out and the 50 Hz ringing persists. This is not to say that the $\bar{K}_3$ term or its limited range is not important in a complete flutter analysis. For reference purposes the angular zone of the fin-fold mechanism and the angular stiffness within this zone are calculated. The total included angle is approximately

$$\theta(\bar{K}_3) = \tan^{-1}\left(\frac{7/32}{\ell - B - \ell_F}\right) \quad , \tag{26}$$

where

ℓ = fin length = 7.6 in.

B = base length = 0.5 in. (steel fin)

ℓ_F = distance from fin tip to point of force application = 0.3 in.

or

$$\theta(\bar{K}_3) = \tan^{-1}\left(\frac{7/32}{7.6 - 0.5 - 0.3}\right) = 1.84°. \tag{27}$$

The angular stiffness is calculated for small angles as:

$$\bar{K}_{3\theta} = \frac{T}{\theta} = \frac{F\ell}{x/\ell} = \frac{\bar{K}_3 x \ell}{x/\ell} = \bar{K}_3 \ell^2 \quad , \tag{28}$$

where x = deflection at distance ℓ from the fin-fold joint due to a force F. The actual value is

$$\begin{aligned} \bar{K}_{3\theta} &= (12 \text{ lb/in})(7.6 - 0.3 - 0.5 \text{ in})^2 \\ &= 81.6 \frac{\text{in-lb}}{\text{rad}} = 1.42 \frac{\text{in-lb}}{\text{degree}} \end{aligned} \tag{29}$$

In summary of paragraph F, it appears that the most important contributor to the 50 Hz fin mode is the fin structure, followed by the fin base, and then the fin shaft. The fin-fold mechanism is important in the sense of systems dynamics, since it is the most compliant member, although effective over a limited range ($\pm$ 0.9°). As such, it could impact the initial excitation required to establish flutter instability.

G. Backlash

Loose motion in the actuator and fin linkage was not made a part of this analysis because a loose or tight fin joint did not measurably affect the 50 Hz mode; even though small, the loose motion was not consistant at the fin/shaft interface among the fins available for testing. This is not to say, however, that backlash would not be a contributive element in establishing a flutter stability margin.

III. CONCLUSIONS

A. The fin-fold mechanism provides the most compliant member but is limited to about $\pm$ 0.9°. Even within this zone the fin-fold mechanism has a stiffness of about 10.3 in/lb/°.

B. Even though the fin-fold mechanism is the most compliant member of the actuator bearing, fin shaft, fin base, fin-fold mechanism, and fin structure series, the large sliding friction causes this bending mode to be highly damped.

C. The predominant mode frequency is about 50 Hz in the $\bar{x}$ and $\bar{z}$ directions - those motions about the two axes perpendicular to the fin shaft axis. This is the frequency range of observed flutter in both MIL No. 5 and in wind tunnel testing, and is most likely the determining element in the flutter frequency.

D. If it were not for friction in the fin-fold mechanism, this joint would determine the natural frequency for small (less than $\pm$ 0.9°) deflections. However, for both small, and more importantly, for large deflections the 50 Hz mode is predominant (the flutter phenomenon resulted in large deflections).

E. The predominant 50 Hz mode results primarily from the series combination of the fin structure and the "radial" type spring of the fin base into which the fin/actuator shaft is inserted. The fin structure is slightly more compliant than the base. The frequency is approximately the same for both steel and aluminum base fins. The amount of loose motion in the shaft/fin-base joint did not affect the predominant mode frequency measurably (less than 1 Hz). However, its effect is to contribute phase lag and therefore would impact flutter stability margin.

F. The Small 49 Hz, 4.2° P-P bursts of motion in the actuator servo noted in MIL No. 6 and in previous flight records is not explained by this analysis. It was first thought that the only partial balancing of the fins in MIL No. 6 could account for coupling of translational motion of the wing into motion about the hinge axis. This was not duplicated in the laboratory, even with the old unbalanced fins. Apparently it takes some added ingredients which causes coupling into the servo axis such as the aiding hinge moment. It is probable that turbulence and buffeting couples considerable energy into the 50 Hz mode and that the combination of fin mass unbalance and aiding hinge moment provides the necessary coupling into the servo axis. Torsional bending of the fin was not considered in this analysis.

G. Servo stiffness and fin stiffness are undoubtably two dimensions of the flutter phenomenon. Quite likely, enough corrective change in the stiffness of any one: servo stiffness at 40 - 60 Hz; fin structural stiffness, perhaps including even torsional stiffness; aiding hinge moment coefficient; or fin mass unbalance could assure a comfortable stability margin for FOG-M flight conditions. A thorough flutter analysis would clearly display these variables. It now appears that the successful early flights did not have much of this stability margin since the servo stiffness of the large pneumatic actuators at 50 Hz was larger than the small actuator used in MIL No. 5 only

by the larger friction and viscous damping coefficient in the large actuator. Percentage wise, this was only a small increase since stiffness at 50 Hz is dominated by the load (fin) inertia. Thus, it is possible that only a small change in one or more of the above design variables would give the desired stablity margin; but until the flutter analysis is complete, a safe course would seem to be either the large or small actuator with balanced fins. The added inertia slightly increases servo stiffness.

H. Another analysis will be conducted which specifically addresses the small signal actuator capability at 48 to 50 Hz.

DISTRIBUTION

	Copies
U. S. Army Materiel System Analysis Activity ATTN: AMXSY-MP Aberdeen Proving Ground, MD 21005	1
IIT Research Institute ATTN: GACIAC 10 W. 35th Street Chicago, IL 60616	1
AMSMI-RD, Dr. McCorkle	1
Dr. Rhoades	1
Dr. Stephens	1
-RD-GC-C	25
-RD-CS-R	15
-RD-CS-T	1
AMSMI-GC-IP, Mr. Bush	1